Active drive towards elastic spinodals

Ayan Roychowdhury,[1,2] Madan Rao,[1] and Lev Truskinovsky[2]

[1] *Simons Centre for the Study of Living Machines, National Centre for Biological Sciences-TIFR, Bengaluru, India 560065.*

[2] *PMMH, CNRS–UMR 7636, PSL-ESPCI, 10 Rue Vauquelin, Paris 75005, France.*

Active matter, exemplified by adaptive living materials such as the actomyosin cytoskeleton, can navigate material parameter space dynamically, leading to unconventional mechanical responses. In particular, it can self-drive toward *elastic spinodal* regimes, where inhomogeneous floppy modes induce elastic degeneracy and enable a controlled interplay between rigidity loss and recovery. Proximity to such marginal states leads to stress localization and the formation of force chains that can be actively assembled and disassembled. Here, we extend the classical notion of spinodal states to active solids and demonstrate how these extreme mechanical regimes can be actively accessed. Moreover, we show that in a nonlinear setting, crossing elastic spinodals generates new energy wells and makes force channeling an intrinsic feature of the emerging microstructure.

1. INTRODUCTION

In passive systems elastic rigidity usually emerges as a result of breaking continuous symmetry [1]. It can also appear in the process of introducing overconstraining interactions [2–6] or as a result of tuning of the pre-stress [5, 7–12]. Similarly, it is known that rigidity can be lost in passive systems due to symmetry restoration [1, 13], through underconstraining [14, 15] and by relaxing the pre-stress [1, 7, 14, 16, 17].

Living materials, operating far from equilibrium, can be more flexible in manipulating the partial loss and recovery of elastic rigidity [1, 7, 14]. This process is often driven by the transduction of metabolic resources into functional work [18–30]. Specifically, active systems can tune their elastic response by modifying their effective energy landscape, thereby, developing soft modes endogenously [28–32]. In particular, due to the presence of activity, the dynamic realizations of fragile matter become possible [15, 33, 34], with marginality successfully maintained despite the fact that the overall stability of the system is compromised [35–38]. One may argue that living systems would be retained in a controlled marginally stable state if the emerging soft modes facilitate function [11, 39–44].

A prototypical context for such behavior is the vast repertoire of rigidities exhibited by the active cellular cytoskeleton [46, 47] whose continuous reconfiguration generates a range of mechanical responses [48, 49]. Behind this remarkable mechanical performance is the activity of molecular motors that can either stiffen the cytoskeleton through actively generated pre-stress or fluidize it by facilitating remodeling [12, 18, 19, 22, 25–27, 50].

A closely related manifestation of the highly nonconventional elastic response in such systems is the emergence of extreme stress and strain concentration which takes the form of force channeling – as, for instance, in actomyosin 'stress fibers' [51, 52] or 'dense tethers' during active remodeling of the extracellular matrix [53–61]. The emerging localized structures can channel forces and can be both assembled and disassembled [62–66]. Ultimately the ability of active systems to generate highly adaptable spatial patterns of densification and alignment is behind long distance mechanotransduction indicating the emergence of mechanical pathways which may be as important as the biochemical ones [12, 67–72].

At the microscopic level, the accessibility of the underlying marginally rigid configurations can be attributed in cytoskeleton to buckling of the constituent semiflexible actin filaments[16], loss of crosslinkers, resulting in their relative sliding [73], to wrinkling [74] and can also be linked to the stretching-to-bending transition [75–79]. The underlying ideas, allowing cytoskeletal systems to maintain the elastically extreme regimes, are currently of considerable interest for the design of artificial biomimetic materials and devices [80–91].

In this paper, we identify some of the strategies that enable active solids to reach elastically degenerate regimes characterized by partial rigidity loss. While such regimes have been explored for passive solids [15, 33, 38, 92–95], we demonstrate how active solids, by tuning their internal activity to navigate the material parameter space, access these states. Additionally, we explore the richness of emerging soft modes by examining inhomogeneous deformations that arise in marginal regimes due to endogenous driving.

Our analysis of the elastically marginal states builds on the concept of *elastic spinodals*, distinguishing them from the conventional *thermodynamic spinodals*. This distinction is due to the presence of long range interactions in elastic systems, arising from the gradient nature of the order parameter and the attendant compatibility constraints [96]. While the conventional thermodynamic spinodals are associated with the appearance of zero eigenvalues of the finite dimensional elastic stiffness matrix [97], *elastic spinodals* emerge due to the appearance of zero eigenvalues of the (infinite dimensional) elastic differential operator [94, 95]. We show that the corresponding inhomogeneous soft modes representing, for instance, incipient force chains, would emerge from internal loading in constrained environments. The latter can be potentially realized in living cells embedded in confluent tissues or attached to patterned substrates [51, 52].

To keep the analysis transparent, we deal with the simplest case of isotropic solids, and address in full detail the accessibility of the corresponding limits of elastic stability. In particular, we classify all finite wave-vector instabilities in such systems. Reaching such stability thresholds usually means termination of an equilibrium branch and indicates a transition from statics to dynamics [94, 95]. The general vectorial criterion of weak local stability is given by the Legendre–Hadamard conditions, related also to ellipticity loss of the equations of elastostatics [92, 98, 99].

The possibility of reaching elastically marginal states, which lie beyond the realm of ordinary materials, has been so far under-emphasized in the literature. In this paper, we show that such states can be realized in active matter. Furthermore, we demonstrate that active systems can potentially cross the *elastic spinodal* thresholds, provided that the model ensures proper stabilization of these marginal states through nonlinear and higher gradient terms. A central focus of this paper is to establish that an important consequence of proximity to marginal thresholds is the emergence of force channeling along transient structures that can be actively assembled and disassembled.

As part of our analysis, we demonstrate that the *macroscopic* active drive toward marginal states is underpinned by a *microscopic* stochastic mechanism that destabilizes certain energy minima while generating new ones in the effective free energy landscape. Specifically, we provide an explicit example of stochastic dynamics in a prototypical system exposed to non-equilibrium noise, which effectively renormalizes linear elastic moduli from positive to negative values.

In summary, our study highlights the adaptive nature of active matter, where endogenous activity can dynamically alter its elastic response. Such 'smart' materials can operate near rigidity thresholds, using a rich spectrum of soft modes to regulate the balance between solidity and fluidity. Moreover, our results suggest that mechanical feedback pathways – capable of being built up and broken down as needed – allow active materials to self-drive toward marginal stability, where partial rigidity loss enables the emergence of non-affine, low-energy 'mechanisms'.

The paper is organized as follows. In Section 2, we focus on linear elastic isotropic solids and show that, by coupling the activity level to the current state of passive stress or strain, the system can renormalize its elastic response in a broad range, potentially reaching both thermodynamic and elastic spinodals. Thermodynamic spinodals are addressed in Section 3 where we discuss the level of elastic degeneracy in such regimes. Section 4 is dedicated to the study of *elastic spinodals* where we address the issue of extreme stress concentration in these regimes and also discuss various approaches allowing one to regularize the emerging singularities. Nonlinear active solids are the subject of Section 5 where we consider in full detail a prototypical model extended beyond the limits of linearized marginality. To complement this largely phenomenological approach, we present in Section 6 a microscopic stochastic model showing how the introduction of a correlated noise can modify the structure of the energy landscape. Finally, in Section 7 we summarize the obtained results and present our conclusions.

2. LINEAR ELASTIC ACTIVE SOLIDS

To elaborate the idea of active accessibility of elastic spinodals it is sufficient to consider the simplest case of an isotropic linear elastic solid in 2D. We start with writing the total stress $\boldsymbol{\sigma}$ (say, of an active meshwork) as a sum of elastic and active terms,

$$\boldsymbol{\sigma} = \mathbb{C}^e \boldsymbol{\epsilon} + \boldsymbol{\sigma}^a. \tag{1}$$

Here, $\boldsymbol{\epsilon} = (\nabla \boldsymbol{u} + \nabla \boldsymbol{u}^T)/2$ is the strain tensor and $\boldsymbol{u}(\boldsymbol{x})$ is the displacement field. The fourth order elastic tensor $\mathbb{C}^e$ has the standard isotropic form,

$$\mathbb{C}^e_{ijkl} = B^e\, \delta_{ij}\delta_{kl} + \mu^e(\delta_{ik}\delta_{jl} + \delta_{il}\delta_{jk} - \delta_{ij}\delta_{kl}), \tag{2}$$

where B^e and μ^e are the passive bulk and shear moduli, respectively.

According to (1), in the presence of activity, the total stress $\boldsymbol{\sigma}$ has an inelastic additive component $\boldsymbol{\sigma}^a$ first introduced in [100, 101]. We consider a special case when the active stress can be represent in the form

$$\boldsymbol{\sigma}^a = \mathbb{A}\boldsymbol{M}, \tag{3}$$

where $\boldsymbol{M}(\boldsymbol{x})$ is a symmetric second order *fabric* tensor field characterizing the density distribution of active agents and encoding, for instance, a locally diffused dipolar mass anisotropy of active elements, such as myosin [102–104] density distribution. The fourth order tensor $\mathbb{A}$ is again assumed to be isotropic

$$\mathbb{A}_{ijkl} = \zeta\, \delta_{ij}\delta_{kl} + \xi\, (\delta_{ik}\delta_{jl} + \delta_{il}\delta_{jk}), \tag{4}$$

where now the coefficients ζ and ξ characterize the levels of spherical and deviatoric activity, respectively.

The constitutive turnover of active elements can be incorporated into the model through the assumption that the anisotropy represented by the tensor $\boldsymbol{M}$ is not arbitrary but is instead enslaved to the anisotropy of the current value of stress. It is implied that the stress state is felt by the fabric and that the latter can be re-orientd in the former. For instance, we assume in this way that stress anisotropy can locally re-orient cytoskeletal meshworks [49, 105, 107–109]. Here it may be also appropriate to mention highly relevant studies of tensegrity models, where load induced stiffening of living cells has been linked to alignment/remodelling of stress fibers along the loading direction [12].

2.1. Stress induced regulation

The simplest quantitative assumption which expresses this type of stress regulation is [102, 103]

$$\boldsymbol{M}(\boldsymbol{x}) = \boldsymbol{M}_0 + \mathbb{L}\boldsymbol{\sigma}(\boldsymbol{x}), \tag{5}$$

where $\boldsymbol{M}_0$ is a constant second order tensor and $\mathbb{L}$ is the fourth order tensor which is again assumed to be isotropic

$$\mathbb{L}_{ijkl} = \bar{L}_b\, \delta_{ij}\delta_{kl} + L_s\, (\delta_{ik}\delta_{jl} + \delta_{il}\delta_{jk}), \tag{6}$$

now with coefficients $\bar{L}_b$ and L_s representing the level of stress-texture coupling. In view of the linearity assumption in (5), we effectively renormalize the isotropic linear elastic moduli.

Indeed, if we eliminate $\boldsymbol{M}$ from the stress-strain relation for the total stress $\boldsymbol{\sigma}$, we obtain

$$\begin{aligned}\boldsymbol{\sigma} &= \mathbb{C}^e\boldsymbol{\epsilon} + \boldsymbol{\sigma}^a = \mathbb{C}^e\boldsymbol{\epsilon} + \mathbb{A}\boldsymbol{M}\\ &= \mathbb{C}^e\boldsymbol{\epsilon} + \mathbb{A}(\boldsymbol{M}_0 + \mathbb{L}\boldsymbol{\sigma}).\end{aligned} \tag{7}$$

After algebraic reorganization, this yields

$$\boldsymbol{\sigma} = (\mathbb{I} - \mathbb{A}\mathbb{L})^{-1}\mathbb{C}^e\boldsymbol{\epsilon} + (\mathbb{I} - \mathbb{A}\mathbb{L})^{-1}\mathbb{A}\boldsymbol{M}_0, \tag{8}$$

which shows that

$$\mathbb{C} = (\mathbb{I} - \mathbb{A}\mathbb{L})^{-1}\mathbb{C}^e \tag{9}$$

can be viewed as activity renormalized linear elastic stiffness tensor; the second term in (8) plays the role of active prestress.

Note that in the cytoskeletal setting, we are essentially postulating in (5) that the tensorial kinetic rate of binding of active crosslinkers $\mathbf{k}^b = k^b\,\mathbf{I}$ is balanced by a Bell-type stress dependent unbinding rate $\mathbf{k}^u\boldsymbol{M}$ with [106, 110–114]

$$\mathbf{k}^u(\boldsymbol{\sigma}) = k^u(\mathbf{I} + e^{\hat{\mathbb{L}}\boldsymbol{\sigma}}), \tag{10}$$

where $\hat{\mathbb{L}}$ is again a standard isotropic forth order tensor characterized by two constant coefficients. Under these assumptions we obtain that in the limit of small stress, $\mathbb{L} = -(k^b/4k^u)\hat{\mathbb{L}}$ and $\boldsymbol{M}_0 = (k^b/2k^u)\mathbf{I}$.

More generally, in the approximation of weak activity, we obtain from (9)

$$\mathbb{C} \approx (\mathbb{I} + \mathbb{A}\mathbb{L})\mathbb{C}^e, \tag{11}$$

where

$$\begin{aligned}&(\mathbb{A}\mathbb{L})_{ijkl} = \mathbb{A}_{ijpq}\mathbb{L}_{pqkl}\\ &= 2\big(\zeta(\bar{L}_b + L_s) + \xi L_s\big)\delta_{ij}\delta_{kl} + 2\xi L_s(\delta_{ik}\delta_{jl} + \delta_{il}\delta_{jk})\\ &=: 2\zeta\tilde{L}_b\,\delta_{ij}\delta_{kl} + 2\xi L_s(\delta_{ik}\delta_{jl} + \delta_{il}\delta_{jk}),\end{aligned} \tag{12}$$

and $\tilde{L}_b := \bar{L}_b + \Big(1 + \frac{\xi}{\zeta}\Big)L_s$. Furthermore, since

$$\begin{aligned}&(\mathbb{A}\mathbb{L}\mathbb{C}^e)_{ijkl} = (\mathbb{A}\mathbb{L})_{ijpq}\mathbb{C}^e_{pqkl}\\ &= 4\big(\zeta\tilde{L}_b(\lambda^e + \mu^e) + \xi L_s\mu^e\big)\delta_{ij}\delta_{kl}\\ &+ 4\xi L_s\mu^e(\delta_{ik}\delta_{jl} + \delta_{il}\delta_{jk}),\end{aligned} \tag{13}$$

the renormalized isotropic elastic moduli take the form

$$B = B^e(1 + 4\zeta L_b), \tag{14}$$

and

$$\mu = \mu^e(1 + 4\xi L_s), \tag{15}$$

where $B^e := \lambda^e + \mu^e$ and

$$L_b := \bar{L}_b + \Big(2 + \frac{\xi}{\zeta}\Big(1 + \frac{\mu^e}{B^e}\Big)\Big)L_s.$$

Note that the sign of $L_{b,s}$ determines whether activity leads to a stiffening or softening of the elastic material.

2.2. Strain induced regulation

In an alternative case when the fabric tensor $\boldsymbol{M}$ is regulated by strain $\boldsymbol{\epsilon}$ (rather than the stress $\boldsymbol{\sigma}$), we can similarly assume that

$$\boldsymbol{M} = \boldsymbol{M}_0 + \mathbb{K}\boldsymbol{\epsilon}, \tag{16}$$

where the tensor $\mathbb{K}$ is again assumed to be isotropic with parameters $K_{b,s}$

$$\mathbb{K}_{ijkl} = \bar{K}_b\,\delta_{ij}\delta_{kl} + K_s\,(\delta_{ik}\delta_{jl} + \delta_{il}\delta_{jk}). \tag{17}$$

Then the effective (renormalized) linear elastic response is

$$\begin{aligned}\boldsymbol{\sigma} &= \mathbb{C}^e\boldsymbol{\epsilon} + \boldsymbol{\sigma}^a = \mathbb{C}^e\boldsymbol{\epsilon} + \mathbb{A}\boldsymbol{M}\\ &= \mathbb{C}^e\boldsymbol{\epsilon} + \mathbb{A}(\boldsymbol{M}_0 + \mathbb{K}\boldsymbol{\epsilon}) = (\mathbb{C}^e + \mathbb{A}\mathbb{K})\boldsymbol{\epsilon} + \mathbb{A}\boldsymbol{M}_0,\end{aligned} \tag{18}$$

In the low activity level limit the renormalized stiffness tensor is

$$\mathbb{C} = \mathbb{C}^e + \mathbb{A}\mathbb{K}, \tag{19}$$

while the second term in (18) again represents active prestress. To obtain the expressions for the renormalized isotropic linear elastic moduli we write

$$\begin{aligned}&(\mathbb{A}\mathbb{K})_{ijkl} = \mathbb{A}_{ijpq}\mathbb{K}_{pqkl}\\ &= 2\big(\zeta(\bar{K}_b + K_s) + \xi K_s\big)\delta_{ij}\delta_{kl} + 2\xi K_s(\delta_{ik}\delta_{jl} + \delta_{il}\delta_{jk})\\ &=: 2\zeta\tilde{K}_b\,\delta_{ij}\delta_{kl} + 2\xi K_s(\delta_{ik}\delta_{jl} + \delta_{il}\delta_{jk}),\end{aligned} \tag{20}$$

where $\tilde{K}_b := \bar{K}_b + \Big(1 + \frac{\xi}{\zeta}\Big)K_s$. The resulting expressions of the effective isotropic elastic moduli are

$$B = B^e + 2\zeta K_b, \tag{21}$$

and

$$\mu = \mu^e + 2\xi K_s, \tag{22}$$

where again $B^e := \lambda^e + \mu^e$ and

$$K_b := \tilde{K}_b + \Big(1 + \frac{\xi}{\zeta}\Big)K_s.$$

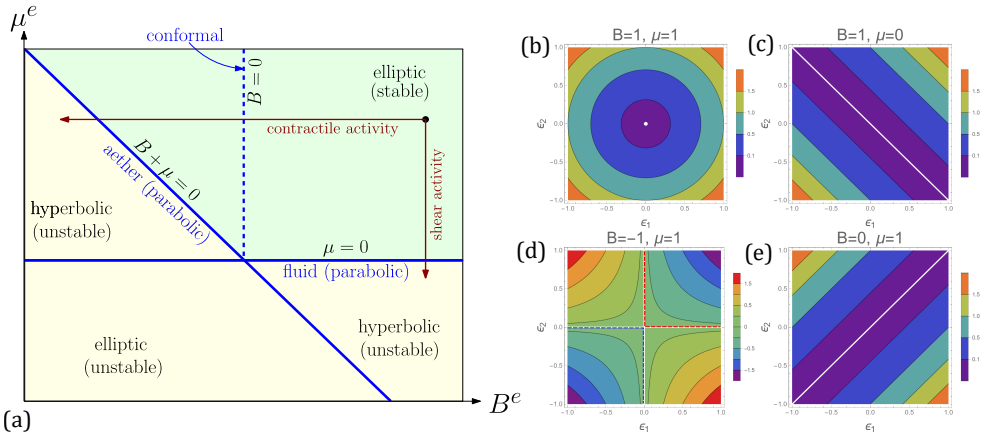

FIG. 1. (a) Regime diagram in the space of elastic moduli for the classical isotropic linear elastic solid. (b-e) Contours of the linear elastic strain energy density $w(\epsilon_1, \epsilon_2)$ for different B and μ; white line indicates zero 'valleys'. In (b) we see a single strain energy minimum. It transforms into a continuous distribution of minima in the thermodynamic spinodal regimes: (c) elastic fluid and (e) conformal material. In (d), we show the two soft mode branches of elastic aether $\det[\boldsymbol{\epsilon}] = 0$: no compression aether: $\mathrm{tr}[\boldsymbol{\epsilon}] > 0$ (red dotted line) and no tension aether: $\mathrm{tr}[\boldsymbol{\epsilon}] < 0$ (blue dotted line).

2.3. Experimental evidence

As we have seen, in the proposed model the effective moduli B and μ can vary in broad limits characterized by the accessible range of the activity coefficients ζ or ξ. Such variations have been indeed recorded in experiments on living systems.

For instance, the implied stiffening or softening response induced by endogenous (active) loading, was observed in crosslinked actin mesh [16, 22, 27, 50, 107, 115–119]. In particular, it was shown that both the effective bulk and shear moduli, B and μ, can stiffen from 1Pa to 100Pa in response to significant increase in motor activity upto 10-30 fold.

Initial softening followed by stiffening of crosslinked actomyosin in solution after activating the motors by ATP addition was observed in [120, 121]. It was shown that after ATP addition, the effective shear modulus μ initially abruptly drops from ∼80 Pa to almost ∼0 Pa due to increased mobility of the elements. At later times, the shear modulus rose to ∼350 Pa as the myosin hydrolyzed the ATP and the formation of rigor bonds with actin filaments took place [120, 121].

To corroborate our assumption of enslavement of the fabric tensor to the local stress/strain state we refer to *in vivo* studies of self-organization of actomyosin cytoskeletal structures in mammalian cells [122] which showed that the dissociation of individual non-muscle myosin IIA filaments takes place with rate $k^u \sim 0.01\, s^{-1}$. On the other hand, the macroscale formation and reorientation dynamics of actomyosin stress fibers depend on factors at several levels of organization, such as crosslinking density and anisotropy, filament stiffness, substrate anchoring and local adaptive regulation mechanisms, and, hence, it is much slower, taking several minutes to hours [51, 52].

Finally, we mention that in the case of 'catch' bonds we may expect that $L_{b,s} < 0$ or $K_{b,s} < 0$ [31, 32, 107]. This suggests that the values of the elastic moduli can potentially reach the elastic stability limits specified in the next Section. However, to corroborate such a possibility at a quantitative level, much more extensive experimental studies would be needed. Those are expected to confirm with certainty the proposed time scale separation and link more securely the increase of endogenous activity in say, actomyosin cytoskeleton, with the attendant changes in the (quasi)elastic properties of the meshwork.

3. THERMODYNAMIC SPINODALS

We recall that reaching thermodynamic spinodal means the loss of convexity of the (activity renormalized) effective energy density viewed as a function of strain tensor $\boldsymbol{\epsilon}$. In the linear elastic setting this is equivalent to the loss of the positive definiteness of the effective elastic stiffness tensor. Note that in the definition of thermodynamic spinodals the constraint of strain compatibility, $\mathrm{curl}\,\mathrm{curl}\,\boldsymbol{\epsilon} = 0$, is irrelevant. This is a consequence of the fact that only homogeneous deformation are taken into account.

In the simplest nontrivial case of a 2D isotropic linear elastic material the elastic energy can be written in the form

$$w(\epsilon_1, \epsilon_2) = B\,(\epsilon_1 + \epsilon_2)^2/2 + \mu\,(\epsilon_1 - \epsilon_2)^2/2, \qquad (23)$$

where the strain tensor is represented by the principal strains $\epsilon_{1,2} := (\mathrm{tr}\,\boldsymbol{\epsilon} \pm \sqrt{(\mathrm{tr}\,\boldsymbol{\epsilon})^2 - 4\det\boldsymbol{\epsilon}})/2$. From (23) it is clear that convexity of energy requires positive definiteness of the moduli, $B > 0$ and $\mu > 0$. These inequalities ensure that the elastic body is stable independently of the type of the boundary conditions. In this sense, they are sufficient but not necessary for elastic stability.

We recall that for isotropic materials in 2D the fourth order elastic stiffness tensor $\mathbb{C}$ can be represented as a 3×3 matrix with eigenvalues $2B$, 2μ and 2μ. To identify the (homogeneous) floppy modes activated at the corresponding thermodynamic stability thresholds (thermodynamic spinodals)

$$B = 0 \tag{24}$$

and

$$\mu = 0 \tag{25}$$

we first observe that at $\mu = 0$ there are two degenerate eigenvalues while at $B = 0$ there is one. It is then easy to see that at the 'elastic fluid' threshold $\mu = 0$ two shear modes soften, while at the 'conformal' threshold $B = 0$ (see the explanation for this term below), a single dilatation mode becomes floppy. We can now illustrate the degeneracies of the energy landscape associated with these two thermodynamic spinodal regimes. In view of the isotropy, it is again convenient to use the space of principal strains (ϵ_1, ϵ_2). Since we are in the linear elastic framework, the implied degeneracies always take the form of a transformation of a single minimum of the quadratic elastic energy at $\epsilon_1 = \epsilon_2 = 0$, see Fig. 1(a), into the zero energy 'valleys' representing continuously degenerate minima. Thus, we obtain a zero dilatation valley

$$\epsilon_1 + \epsilon_2 = 0 \tag{26}$$

in the case of an elastic fluid which can be then viewed as a 'unimodal material' and a zero shear valley

$$\epsilon_1 - \epsilon_2 = 0 \tag{27}$$

in the case of dilatation-insensitive (conformal) solid which is then a 'bimodal material', see Fig. 1(c,e). We use here the language of unimodal and bimodal materials taken from the theory of composite materials [81].

To illustrate the emergence of inhomogeneous soft modes at the thermodynamic spinodals it is sufficient to consider the threshold $B = 0$. As we have seen in such a limiting regime, purely dilatational deformations with $\epsilon_{xx} - \epsilon_{yy} = 0$ and $\epsilon_{xy} = 0$ cost no energy. If we express these conditions in terms of displacements, we obtain

$$\begin{aligned} u_{x,x} &= u_{y,y}, \\ u_{x,y} &= -u_{y,x}. \end{aligned} \tag{28}$$

In view of (28), the two components of the displacement field (u_x, u_y) are both harmonic functions. Moreover,

$$\nabla \boldsymbol{u} = \begin{pmatrix} u_{y,y} & -u_{y,x} \\ u_{y,x} & u_{y,y} \end{pmatrix} = \mathbf{R}\mathbf{U} \tag{29}$$

where

$$\mathbf{U} = \sqrt{a^2 + b^2}\mathbf{I}$$

is a pure dilatation with $a = u_{y,y}$, $b = u_{y,x}$, and $\mathbf{R}$ is a rotation by angle $\tan^{-1}(b/a)$. Such purely dilatational inhomogeneous soft displacement modes are then angle preserving. It is in view of these features, that the material with $B = 0$ is called the conformal material [82, 123].

Note also that the stress in a 'conformal' solid is necessarily trace free,

$$\mathrm{tr}[\boldsymbol{\sigma}] = 0. \tag{30}$$

This makes the force balance problem

$$\mathrm{div}\, \boldsymbol{\sigma} = \mathbf{0}, \tag{31}$$

statically determinate (isostatic) [15, 69, 124–127].

While the equations of elasticity remain elliptic at the conformal threshold $B = 0$, the elastic body still becomes unstable in the presence of an unconstrained part of the boundary. This is because of the failure of the 'complementing condition' at $B = 0$, which marks the effective 'loss of ellipticity on the boundary' [128]. This means, for instance, that for a solid body with $B = 0$ the traction free boundary is always unstable against surface wrinkling of the form

$$\boldsymbol{u}(\boldsymbol{x}) = Re[\boldsymbol{z}(s)e^{i\mathbf{q}\cdot\boldsymbol{x}}], \tag{32}$$

where $\mathbf{q}$ is an arbitrary wave vector representing lateral wiggles while the function

$$\boldsymbol{z}(s) = \mu(iq\,\boldsymbol{\nu} + \mathbf{q})e^{-qs} \tag{33}$$

describes the exponential decay away from the free surface. Here $\boldsymbol{x}$ is a spatial coordinate on the (free) surface with normal $\boldsymbol{\nu}$ and s is the coordinate perpendicular to this surface [129]. Since any unconstrained segment of the boundary can be expected to undergo a surface instability as the limit $B = 0$ is reached, active materials with free boundaries, e.g., cells in suspension [130], are potentially susceptible to such instabilities [39, 86, 129, 131]. It is interesting that despite the presence of these instabilities, thermodynamic spinodals, corresponding to both $\mu = 0$ and $B = 0$, have been successfully achieved by meta-material constructions [81–87, 132–138].

4. ELASTIC SPINODALS

Next we define the *elastic spinodals* while remaining in the simplest setting of 2D isotropic linear elasticity. If we Fourier transform the Navier's equilibrium equations:

$$\mathrm{div}\, \boldsymbol{\sigma} = \mu\, \nabla^2 \boldsymbol{u} + B\, \nabla(\mathrm{div}\, \boldsymbol{u}) = 0, \tag{34}$$

we obtain

$$\mathbf{Q}(\mathbf{q})\, \hat{\boldsymbol{u}}(\mathbf{q}) = \mathbf{0}, \tag{35}$$

where

$$\hat{\boldsymbol{u}}(\mathbf{q}) = (1/2\pi) \int_{\mathbf{R}^2} \boldsymbol{u}(\boldsymbol{x})\, e^{-2\pi i\, \boldsymbol{x}\cdot\mathbf{q}}\, d\boldsymbol{x}.$$

In (35) we introduced the acoustic tensor [98, 139]

$$\mathbf{Q}(\mathbf{q}) = (B+\mu)\,\mathbf{q}\otimes\mathbf{q} + \mu(\mathbf{I}-\mathbf{q}\otimes\mathbf{q}). \tag{36}$$

In terms of acoustic tensor we can formulate the conditions of elastic marginality in the form

$$\det \mathbf{Q}(\mathbf{q}) = 0. \tag{37}$$

In view of (37) marginality is defined here as the condition when at least one of the eigenvalues of the elasticity operator (35) is equal to zero.

It is straightforward to see that the condition (37) is satisfied whenever either

$$\mu = 0 \tag{38}$$

or

$$B+\mu = 0 \tag{39}$$

The conditions (38, 39) can be then interpreted as defining the *elastic spinodal* limits [92, 94, 95].

Note that reaching the thresholds (38, 39) indicates that our Navier's equations (34) lose their conventional elliptic nature. As we show below, they also and signal that the character of stress propagation undergoes a fundamental change [98, 99, 139–144].

We further observe that the threshold (38) corresponds to the state where the material has just lost shear resistance and in what follows we refer to such regimes as "elastic liquids". In contrast, at the second threshold (39) it is the resistance to longitudinal deformation that is lost and in what follows, respecting a long tradition [99, 145, 146], we refer to such regimes as "elastic aethers".

Note further that the stability limits (38, 39), which we illustrate in Fig. 1(d), are necessarily weaker than the limits (24, 25) delineating thermodynamic spinodals. We reiterate that the reason is that the latter deal only with homogeneous (affine, finite dimensional) perturbations while the former address a much broader class of inhomogeneous (non-affine, infinite dimensional) perturbations. In particular, only the thresholds (38, 39) account for the gradient nature of the order parameter (strain tensor) and the corresponding elastic compatibility constraints. Therefore thermodynamic spinodals always lie inside the *elastic spinodals*. As we have already seen, the elastic regimes located between the elastic and the thermodynamic spinodals, where the material respect the strong ellipticity conditions while violating the thermodynamic stability conditions, are stable only as long as their boundary is fully constrained [129, 147]. Therefore an artificial synthesis of non-biological materials reaching the *elastic spinodals* remains highly challenging, even though some design ideas for spinodal metamaterial with $B+\mu=0$, which is peculiar due to its 'infinitely auxetic' response, have been already proposed in the literature, e.g. [80].

To understand the physical consequences of having an active material at the *elastic spinodal* limits, we observe that due to the scale-free nature of continuum elasticity, at these thresholds all wavelengths become unstable simultaneously [123, 148]. Therefore the ensuing instabilities are massive: in the elastic liquid regime ($\mu = 0$) the emerging soft modes are all solenoidal fields

$$\operatorname{div} \boldsymbol{u} = 0. \tag{40}$$

Similarly, in the case of elastic aether regime ($B+\mu = 0$), the emerging soft modes are comprised of all irrotational fields

$$\operatorname{curl} \boldsymbol{u} = \mathbf{0}. \tag{41}$$

Note also that the mechanical response at *elastic spinodals* becomes isostatic (jammed, critical) [69]. Specifically, in the elastic liquid regime the deviatoric stress must necessarily vanish

$$\boldsymbol{\sigma} - (1/2)\mathrm{tr}[\boldsymbol{\sigma}]\,\mathbf{I} = \mathbf{0}. \tag{42}$$

Similarly, in the elastic aether regime the determinant of the stress tensor must necessarily vanish

$$\det[\boldsymbol{\sigma}] = 0. \tag{43}$$

We recall that in isostatic states the system is highly coordinated so that both, the nontrivial zero modes and the states of self-stress, are only marginally constrained.

4.1. Green's functions

The tendency towards the formation of displacement discontinuities in *elastic spinodal* regimes can be illustrated most simply by the special structure of the corresponding 2D Green's functions.

To this end, consider the response of an infinite linear elastic body subject to concentrated forces. In the Fourier space the Green's function is just the inverse of the elastic acoustic tensor and in the case of 2D isotropic linear elasticity, characterized by parameters B and μ, we obtain [149]

$$\begin{aligned}\hat{G}_{ij}(q_x,q_y) &= [B\,q_iq_j + \mu\,q_kq_k\,\delta_{ij}]^{-1} \\ &= \begin{bmatrix} \frac{\mu q_x^2+(B+\mu)q_y^2}{\mu(B+\mu)(q_x^2+q_y^2)^2} & -\frac{Bq_xq_y}{\mu(B+\mu)(q_x^2+q_y^2)^2} \\ -\frac{Bq_xq_y}{\mu(B+\mu)(q_x^2+q_y^2)^2} & \frac{(B+\mu)q_x^2+\mu q_y^2}{\mu(B+\mu)(q_x^2+q_y^2)^2} \end{bmatrix}.\end{aligned} \tag{44}$$

In real space, the obtained result can be illustrated by presenting a displacement field generated by a pure shear quadrupole at the origin. Suppose that the latter involves a contractile dipole along the x-axis generated by the point forces $\mathbf{f}^{(1)} = (1,0)$ and $\mathbf{f}^{(2)} = (-1,0)$ which act at the points $(\mp 1, 0)$, respectively, and an extensile dipole along the y-axis, generated by the point forces $\mathbf{f}^{(3)} =$

$(0,-1)$ and $\mathbf{f}^{(4)}=(0,1)$ which act at the points $(0,\mp 1)$. The ensuing displacement field takes the form,

$$\begin{aligned}\boldsymbol{u}(x,y) &= \boldsymbol{u}^{(1)}(x+1,y)+\boldsymbol{u}^{(2)}(x-1,y)+ \quad (45)\\ &+ \boldsymbol{u}^{(3)}(x,y+1)+\boldsymbol{u}^{(4)}(x,y-1), \quad (46)\end{aligned}$$

where the corresponding displacement components are

$$u_x^{(\alpha)}(x,y)=G_{xx}(x,y)f_x^{(\alpha)}+G_{xy}(x,y)f_y^{(\alpha)}, \quad (47)$$

and

$$u_y^{(\alpha)}(x,y)=G_{xy}(x,y)f_x^{(\alpha)}+G_{yy}(x,y)f_y^{(\alpha)}, \quad (48)$$

where $\alpha\in[1,4]$ and the real space Green's functions $G_{ij}(x,y)$ are given by (see, for instance , [150])

$$\begin{aligned}G_{xx}(x,y) &= \frac{1}{4\pi}\Bigg[-\frac{1}{2}\Big(\frac{1}{\mu}+\frac{1}{B+\mu}\Big)\log(x^2+y^2)\\ &\quad +\Big(\frac{1}{\mu}-\frac{1}{B+\mu}\Big)\frac{x^2}{x^2+y^2}\Bigg],\\ G_{xy}(x,y) &= \frac{1}{4\pi}\Big(\frac{1}{\mu}-\frac{1}{B+\mu}\Big)\frac{xy}{x^2+y^2},\\ G_{yy}(x,y) &= \frac{1}{4\pi}\Bigg[-\frac{1}{2}\Big(\frac{1}{\mu}+\frac{1}{B+\mu}\Big)\log(x^2+y^2)\\ &\quad +\Big(\frac{1}{\mu}-\frac{1}{B+\mu}\Big)\frac{y^2}{x^2+y^2}\Bigg]. \quad (49)\end{aligned}$$

The regular case, when the elasticity equations remain elliptic, is illustrated in Fig. 2(a). The singular behavior of the functions (49) at *elastic spinodal* limits $B+\mu\to 0$ and $\mu\to 0$ is shown in Fig. 2(b,c), see also [151–153]. The developing jump discontinuities, as either the elastic aether or the elastic liquid limits are approached, point towards the unavoidable reduced smoothness of the limiting equilibrium fields.

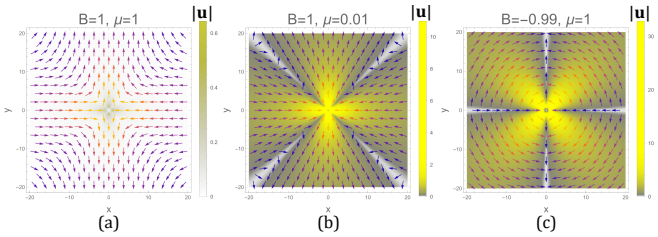

FIG. 2. Elastic response to a force quadrupole placed in an infinite domain in (a) the stable regime, and in the (b,c) elastic spinodal regimes. The displacement field $\mathbf{u}$, is represented by its direction (arrows) and magnitude (color) in (a) the stable material, (b) close to the elastic liquid regime, and (c) close to the elastic aether regime, which show the formation of the localized singularities of the displacement field $\mathbf{u}$.

4.2. Singular stress fields

To emphasize the ubiquity of stress concentration phenomena at *elastic spinodals*, we now recast the isostatic conditions (42) and (43) in terms of classical Airy stress function $\sigma_{xx}=\partial^2_{yy}\chi$, $\sigma_{yy}=\partial^2_{xx}\chi$, $\sigma_{xy}=-\partial^2_{xy}\chi$.

We recall that in the case of elastic aether ($B+\mu=0$) the iso-energy lines $\epsilon_1=0$ and $\epsilon_2=0$ in Fig. 1(d) represent the floppy configurations of the reference state. This degeneracy of the energy landscape implies that either of the two principal stresses is zero, so $\sigma_1\sigma_2=0$. This means that the stress field $\boldsymbol{\sigma}$ is necessarily uniaxial. This property is ultimately behind the isostaticity of this limit suggesting that the equilibrium problem is statically determinate. We recall that in this limit the stress distribution can be indeed found without invoking any notion of strain field using the equations

$$\operatorname{div}\boldsymbol{\sigma}=\mathbf{0}, \qquad \det[\boldsymbol{\sigma}]=0. \quad (50)$$

Using Airy stress function we can reduce this system to a *degenerate-elliptic* Monge-Ampère equation for χ:

$$\partial^2_{xx}\chi\,\partial^2_{yy}\chi-(\partial^2_{xy}\chi)^2=0. \quad (51)$$

The equation (51) is known to admit (static) shock wave type solutions with discontinuous gradients of the Airy function χ [133, 154–156]. In fact, the equation (51) can be solved geometrically and it is known that its general solution contains piecewise smooth developable surfaces with zero Gaussian curvature, linked through folds which can also form corners with singular Mean and Gaussian curvatures [154, 157]. The folds would then indicate the locations of stress channeling [155, 157, 158]. Note that the same folds are also indicative of the presence of displacement discontinuities $[\![\boldsymbol{u}]\!]\neq 0$ suggesting, for instance, the emergence of self penetration.

Finally, we stress that equation (51) *does not* automatically imply the classical strain compatibility condition

$$\operatorname{curl}\operatorname{curl}\boldsymbol{\epsilon}=0,$$

which in terms of Airy function χ would have been equivalent to an elliptic biharmonic equation

$$\nabla^4\chi=0.$$

Therefore the solution of (51) may be incompatible in the sense that for such solutions, representing, for instance, an energy-free, 'inelastic' self penetration, a global reference state would not exist.

In the case of the elastic liquid ($\mu=0$) the degeneracy of the reference state leads to the requirement that the deviatoric part of the stress field $\boldsymbol{\sigma}$ is zero (see the degenerate energy line $\epsilon_1=-\epsilon_2$ in Fig. 1(c)). Therefore the stress equilibrium problem, which is again statically determinate, can be closed as follows

$$\operatorname{div}\boldsymbol{\sigma}=\mathbf{0}, \qquad \operatorname{dev}[\boldsymbol{\sigma}]=\mathbf{0}. \quad (52)$$

Indeed, invoking the Airy stress function χ we obtain the second order hyperbolic system

$$\partial^2_{xx}\chi - \partial^2_{yy}\chi = 0, \qquad \partial^2_{xy}\chi = 0. \tag{53}$$

The two scalar equations (53) describe the independent shear modes associated with the strain variables $\epsilon_{xx} - \epsilon_{yy}$ and ϵ_{xy}. They simultaneously become floppy in our isotropic model ensuring that in equilibrium necessarily $\sigma_{xx} - \sigma_{yy} = 0$ and $\sigma_{xy} = 0$, see the second equation in (52).

As is well known, in hyperbolic systems boundary conditions specified on non-characteristic curves 'propagate' along the characteristics. The first equation in (53) has characteristics $x \pm y = const$; its general solution is therefore of the form $\chi_1(x, y) = f_1(x+y) + g_1(x-y)$. The second equation in (53) has characteristics parallel to the coordinate lines $x = const$ and $y = const$. These characteristics are orthogonal to the family of characteristics of the first equation (53): the corresponding general solution is of the form the form $\chi_2(x, y) = f_2(x) + g_2(y)$. When the the functions $f_{1,2}(x)$ and $g_{1,2}(y)$ are non-smooth, the corresponding surfaces $\chi_1(x, y)$ and $\chi_2(x, y)$ will have folds 'propagating' along the characteristics. The corresponding singularities of either Gaussian or mean curvature or both would then indicate the location of singular stress fields.

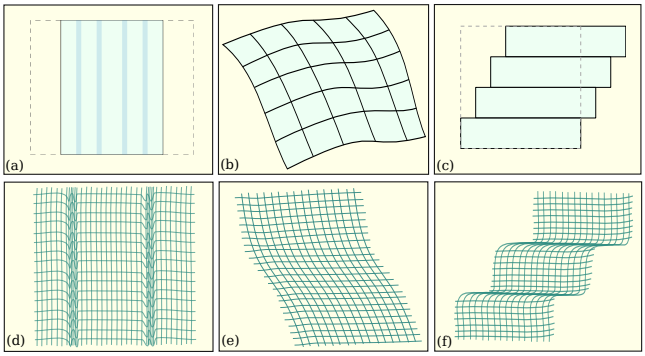

FIG. 3. Schematic representation of the singular mechanical response on *elastic spinodals*. Reference configuration (dashed line) transforms to: *folded* configuration in the elastic aether regime (a); *smooth* configuration in the elastically stable regime, $\mu > 0, B + \mu > 0$ (b); *slipped* configuration in the elastic liquid regime (c). (d,e,f) Corresponding regularized displacement fields.

To summarize, in both cases of the elastic aether ($B + \mu = 0$) and the elastic liquid ($\mu = 0$) the system of governing equations admits (static) shock-wave-type solutions with discontinuous gradients of the Airy function $\chi(\boldsymbol{x})$, indicating the presence of displacement jumps $[\![\boldsymbol{u}]\!] \neq 0$. Outside the corresponding sharp folds elasticity remains non-degenerate, the function χ remains smooth and elastic compatibility holds.

To understand the physical meaning of the discontinuous displacement field we can mention that in the case of elastic liquids the emerging jumps would reflect a formation of slip lines, see Fig. 3(c). For elastic liquids similar singular solutions with localized displacement discontinuities are usually discussed in the dynamic framework as weak solutions of Euler equations containing vortex sheets and other singular structures, e.g. [159–164]. Instead, in the case of elastic aethers displacement discontinuities may describe either an internal folding of the material, see Fig. 3(a), or represent an internal unfolding. In this sense the elastic aether can perform mechanically as either a 'no tension' material [165–171] and a 'no compression' material [156, 172–175].

4.3. Fragile nature of elastic spinodals

As we have already seen, to reach an elastic spinodal state in a body with finite geometry requires constraints on the boundaries, such as in living cells belonging to confluent tissues, and in cells adhered on micro-patterned substrates [51]. In both cases the emergence of system-spanning 'force chains' would depend on the anchoring at the cell boundaries (through focal adhesions [176] or at adherens junctions [177]). Since an arbitrary distribution of the anchoring sites would not in general be compatible with the equilibrium structure of the force chain network, a dynamic reorganization of the anchoring configurations and a concomitant reconfiguration of the force chains in the bulk, could be expected until a stable force chain network, compatible with the boundary anchoring distribution, is established [33]. Such intermittent mechanical adjustments through building and dismantling of load supporting sub-structures, has been indeed recorded in mechanically fragile living systems [178–180].

In the case of elastic aether the implied bulk-boundary correspondence can be linked to the fact that the effective energy density

$$w(\boldsymbol{\epsilon}) = \int_0^{\boldsymbol{\epsilon}} \boldsymbol{\sigma}(\boldsymbol{\epsilon}') \cdot d\boldsymbol{\epsilon}' \tag{54}$$

is a null-Lagrangian [181, 182]. Indeed, one can see that

$$\int_\Omega w(\boldsymbol{\epsilon})\, dA = \int_{\partial\Omega} \tau_a(\boldsymbol{u}, \nabla\boldsymbol{u}, \boldsymbol{\nu})\, dx \tag{55}$$

where

$$\tau_a(\boldsymbol{u}, \nabla\boldsymbol{u}, \boldsymbol{\nu}) = -\mu\, e_{ik} e_{jl} \partial_i u_j\, u_k \nu_l \tag{56}$$

is a 'live load' type surface energy, e_{ij} is the Levi-Civita symbol, and $\boldsymbol{\nu}$ denotes the unit normal to the boundary.

In the case of elastic liquid, stress is hydrostatic and the equilibrium problem reduces to finding a distribution of scalar pressure in the bulk. The pressure in the bulk is fully controlled by the pressure distribution on the boundary, which must be spatially constant for static situations. Once again we see that an arbitrary boundary loading is not, in general, compatible with equilibrium

configuration, requiring a dynamic adjustment. More specifically, for elastic fluids the direct link between the bulk and the surface at equilibrium can be illustrated by the straightforward identity

$$\int_\Omega w(\boldsymbol{\epsilon})\, dA \equiv \int_\Omega \frac{B}{2}\partial_i u_i\, \partial_j u_j\, dA = \int_{\partial\Omega} \tau_f(\boldsymbol{u}, \nabla\boldsymbol{u}, \boldsymbol{\nu})\, dx, \tag{57}$$

where the 'live load' type surface energy is now

$$\tau_f(\boldsymbol{u}, \nabla\boldsymbol{u}, \boldsymbol{\nu}) = (B/2)\partial_i u_i\, u_j \nu_j. \tag{58}$$

One can see that in equilibrium, when $\partial_i u_i = \text{const}$, the energy depends only on the imposed change of the total volume while all other types of loading are accommodated dynamically.

We emphasize that such effectively 'holographic' response [183], realized in particular cases through system spanning stress singularities, but mediated in general by the presence of inhomogeneous (collective) soft modes [87, 88, 182], highlights the fragile nature of the mechanical response at *elastic spinodals* [15, 36, 37]. It has been argued that in the case of cytoskeleton, such fragility may be supported by cellular machinery generating transient tensegrity like networks of 'stress fibers' [12, 51, 184].

4.4. Regularized models

In Fig.3(a-c) we illustrated schematic structure of the generic mechanical response on elastic spinodals, showing separately (a) the potentially singular response in elastic aether regime, $B + \mu = 0$; (b) the non-singular conventional regime $\mu > 0$, $B + \mu > 0$; (c) the potentially singular elastic liquid regime, $\mu = 0$. To analyze the mechanical response further, we need to regularize these emergent singularities. We note that the singularities appear in elastic aether and elastic liquid regimes because the underlying continuum theories suffer from two types of problems: (i) they are scale free, and (ii) they are elastically degenerate. Therefore, to regularize such singular response one can either bring into the theory an internal (finite) length scale, or compromise the degeneracy.

In Fig. 3, we provide an illustrative example of the first type of regularization. Our schematics in the panels (d-f) show the same characteristic deformation patterns as in panels (a-c) but in a regularized model containing a small internal length scale. In such model an elastic aether regime would be characterized by small but finite size strain localization replacing singular folds. Elastically non-degenerate regime would be again described by smooth maps which would be basically unchanged vis-à-vis the non-regularized model. Finally, in the elastic liquid regime singular slips would turn into finite size shear bands. The implied 'rounding' of the displacement discontinuities can be achieved by switching from local to nonlocal theory, for instance, by bringing into the model higher gradient elasticity (which we discuss in detail later). Another option would be to replace the continuum model by the discrete one. For comparison of these two approaches to finite length scale regularization, see for instance [185, 186].

We now consider the second type of regularization provided by a conventional linear elastic model which degenerates (saturates) after small but finite deformation takes place [187]. To illustrate the idea, we present here a simple example.

Consider a 1D elastic bar, fixed at both ends, i.e., with $u(0) = u(L) = 0$, where $u(x)$ is the displacement field and L is the reference length of the bar. Suppose that such bar is subjected to a concentrated force f at its center, see Fig. 4(a). Suppose further that the material of the bar is 'active' in the sense that a passive linear elastic response at small strain (characterized by the modulus k), is followed by an activity-induced stress saturation in both tension and compression. We assume that the saturation takes place at $\sigma = \pm\sigma_0$, see Fig. 4(b).

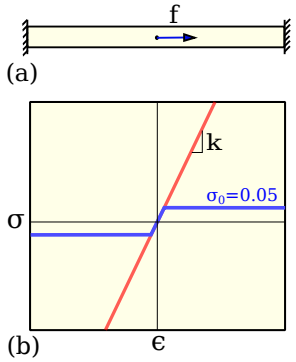

FIG. 4. Strain localization in a loaded active elastic bar: (a) Loading by a body force f at the centre of the clamped bar. (b) Stress-strain relation of the bar with stiffness k (red line) and stress saturation at $\sigma_0 = 0.05$ (blue).

In this model, the fully degenerate *elastic spinodal* limit is reached in the limit $\sigma_0 \to 0$ when non-degenerate elastic range disappears; in the opposite limit, $\sigma_0 \to \infty$, the material behaves as a passive, purely linear elastic medium with a positive stiffness $k > 0$. We stress that, in contrast to the models with an internal length scale, the regularization of a material at the *elastic spinodal* through the introduction of small but finite σ_0, does not directly 'round' singularities, with stress concentration taking place only in the limit of large enough L. As we see in the next section, this mechanism of regularization appears naturally in a theory of a nonlinear active solid that includes binding/unbinding kinetics of myosin.

Turning back to our example, in the trivial non-degenerate linear elastic limit $\sigma_0 \to \infty$ the displacement field is piece-wise linear without showing any signs of localization,

$$u(x) = \begin{cases} \frac{f}{2k}x, & 0 \le x \le \frac{L}{2} \\ \frac{f}{2k}(L - x), & \frac{L}{2} \le x \le L \end{cases}. \tag{59}$$

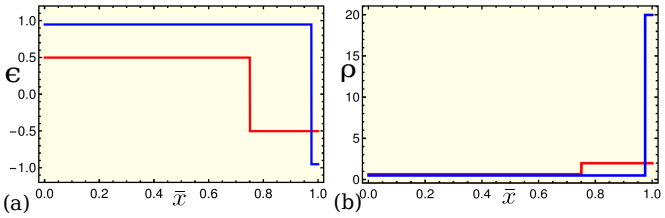

FIG. 5. (a) Strain field $\epsilon = du/dx$, corresponding to Fig. 4, in actual coordinates $\bar{x} = x + u(x)$. (b) The deformed material density $\rho(x) = 1/(1+\epsilon(x))$. Parameters $k = 1$, $f = 1$, $\sigma_0 = 0.05$.

The corresponding strain field $\epsilon = du/dx$ is then

$$\epsilon(x) = \begin{cases} \frac{f}{2k}, & 0 \le x \le \frac{L}{2} \\ -\frac{f}{2k}, & \frac{L}{2} \le x \le L \end{cases} . \tag{60}$$

It is instructive to consider the density field of the deformed material (assuming that the uniform density of the reference material is 1), defined as

$$\rho(x) = \frac{1}{1+\epsilon(x)}, \tag{61}$$

and express it in the actual (deformed) configuration as $\rho = \rho(\bar{x})$ where

$$\bar{x}(x) = x + u(x). \tag{62}$$

Explicitly,

$$\rho(\bar{x}) = \begin{cases} \left(1+\frac{f}{2k}\right)^{-1}, & 0 \le \bar{x} \le \frac{L}{2}\left(1+\frac{f}{2k}\right) \\ \left(1-\frac{f}{2k}\right)^{-1}, & \frac{L}{2}\left(1+\frac{f}{2k}\right) \le \bar{x} \le L \end{cases} . \tag{63}$$

We note that the magnitude of the force f must satisfy the strict inequality $f < 2k$, so that the deformed length of the right segment of the point of application of the force is non-zero. The corresponding profiles are illustrated in Fig. 5 (red lines) for $f = k = 1$ and $L = 1$. Consider next the case when the stress threshold is finite $0 < \sigma_0 < \infty$. Though the resulting equilibrium problem is nonlinear, it can be solved analytically. In particular, the displacement field becomes

$$u(x) = \begin{cases} \frac{f-\sigma_0}{k}x, & 0 \le x \le \frac{L}{2} \\ \frac{f-\sigma_0}{k}(L-x), & \frac{L}{2} \le x \le L \end{cases} . \tag{64}$$

The corresponding strain field $\epsilon(x)$ and deformed density field in the actual configuration $\rho(\bar{x})$ are

$$\epsilon(x) = \begin{cases} \frac{f-\sigma_0}{k}, & 0 \le x \le \frac{L}{2} \\ -\frac{f-\sigma_0}{k}, & \frac{L}{2} \le x \le L \end{cases} , \tag{65}$$

and

$$\rho(\bar{x}) = \begin{cases} \left(1+\frac{f-\sigma_0}{k}\right)^{-1}, & 0 \le \bar{x} \le \frac{L}{2}\left(1+\frac{f-\sigma_0}{k}\right) \\ \left(1-\frac{f-\sigma_0}{k}\right)^{-1}, & \frac{L}{2}\left(1+\frac{f-\sigma_0}{k}\right) \le \bar{x} \le L \end{cases} . \tag{66}$$

Finally, we consider the limit $\sigma_0 \to 0$, when the elastic range around the reference state $\epsilon = 0$ vanishes and the resulting stress strain curve becomes completely flat (*elastic spinodal* regime). For $f = k = 1$, we note that in this limit, the length of the segment on the right of the point of application of the force f, goes to zero

$$L - \frac{L}{2}\left(1+\frac{f-\sigma_0}{k}\right) = \frac{L}{2}\sigma_0 \to 0\,. \tag{67}$$

However, the density (66) inside this segment of the bar tends to infinity

$$\rho = \left(1-\frac{f-\sigma_0}{k}\right)^{-1} = \sigma_0^{-1} \to \infty\,, \tag{68}$$

while the density in the rest of the bar remains small

$$\rho = \left(1+\frac{f-\sigma_0}{k}\right)^{-1} = (2-\sigma_0)^{-1} \to 1/2\,. \tag{69}$$

To summarize, in the *elastic spinodal* limit $\sigma_0 \to 0$, the density profile $\rho(\bar{x})$ localizes around the right boundary. Accordingly, the strains in the left and the right segments, tend to the limits

$$\pm\frac{f-\sigma_0}{k} = \pm(1-\sigma_0) \to \pm 1\,. \tag{70}$$

As a result, the material of the bar concentrates around one point while forming an effective rarefied void-like state everywhere else, see blue line in Fig. 5(b).

We interpret this 1D example as perhaps the most elementary demonstration of the emergence of 'force punctae' in the *elastic spinodal* limit. In 2D at the elastic aether limit, one can expect a similar tendency towards fraying (fragmentation) with a homogeneous state turning into a collection of sparsely distributed dense 'force chains', see also [188].

5. NONLINEAR ELASTIC ACTIVE SOLIDS

While the analysis so far has been restricted to linear elastic response, it is imperative to understand active *elastic spinodals* in a nonlinear setting. This is best realised in the kinetic model, which relates the fields $\boldsymbol{M}$ and $\boldsymbol{\epsilon}$ via a Bell-type relation. Our main finding is that without assuming weak activity, the renormalized stress-strain response becomes inherently nonlinear and may even turn nonmonotonic. In this case, the *elastic spinodal* thresholds, isolated in strain space, can be still reached actively, enabling access to entirely new states disappearing if activity is suppressed.

5.1. 1D Model

To build intuition, we begin with the simplest case and consider a 1D elastic medium carrying a scalar fabric-field $M(x,t)$ (as say, associated with myosin density).

Suppose further that this field is fully enslaved to the evolving strain field $\epsilon(x,t)$. Under this assumption, the equation of chemical balance in the binding-unbinding reaction for the field $M(x,t)$ takes the form,

$$k^b - k^u(\epsilon)M = 0, \tag{71}$$

where k^b is the binding rate which we assume to be strain independent. We take the unbinding rate k^u to be strain dependent with a Bell-form

$$k^u(\epsilon) = k_0^u(1 + e^{K\epsilon}), \tag{72}$$

where k_0^u is a constant. The sign of K determines whether the fabric field exhibits a 'slip bond' ($K < 0$) or a 'catch bond' ($K > 0$) response [107], see Fig. 6(a,b).

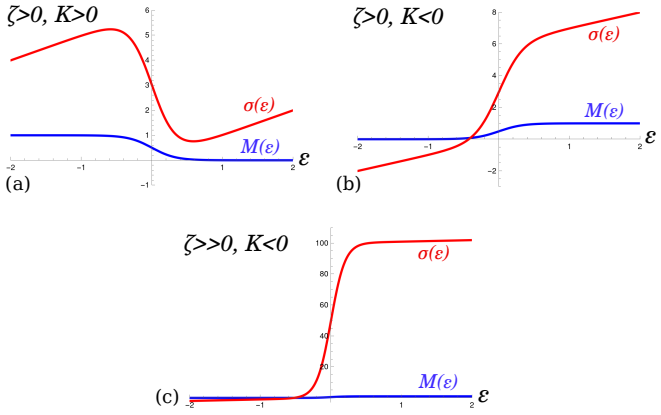

FIG. 6. (a) Non-monotonic stress strain behaviour and 'catch bond' response at small strains, with saturation at large $|\epsilon|$, of the contractile actomyosin bond for $K > 0$. (b) Monotonic stress strain behaviour and 'slip bond' response at small strains, with saturation at large $|\epsilon|$, of the contractile actomyosin bond for $K < 0$. (c) The slip bond response $K < 0$ at large activity $\zeta \gg 0$ (here, $\zeta = 100$, $K = -10$), tending to the active material with finite elastic range set by a stress threshold σ_0.

The relations (71) and (72) give rise to the renormalized nonlinear (quasi)elastic mechanical response, with the following stress-strain relation

$$\sigma \;=\; \mu^e\epsilon + \zeta\, M = \mu^e\epsilon + M_0\zeta(1 + e^{K\epsilon})^{-1}\,. \tag{73}$$

In the 'slip bond' case ($K < 0$), the stress-strain curve $\sigma(\epsilon)$ remains monotonic with a positive tangent modulus $\sigma'(\epsilon) > 0$, ensuring stability (Fig. 6(b)). At high activity $\zeta \gg 0$, this behavior resembles (asymptotically) the response adopted in the regularized model discussed previously, where a linear elastic range at small strain terminated in abrupt stress saturation (Fig. 6(c)). In the 'catch bond' case ($K > 0$), the stress-strain curve $\sigma(\epsilon)$ becomes non-monotonic, with a negative tangent modulus $\sigma'(\epsilon) < 0$ near the reference state, leading to instability (Fig. 6(a)). Consequently, at sufficiently high activity of catch bond type, the effective non-equilibrium energy develops a double-well form, destabilizing the homogeneous state $\epsilon = 0$. This leads to an elastic decomposition into contracted ($\epsilon < 0$) and stretched ($\epsilon > 0$) configurations with high and low densities, respectively.

5.2. Multidimensional extension

In the full tensorial model we need to characterize similar strain control, using the fabric tensor $\boldsymbol{M}(\boldsymbol{x},t)$. The corresponding 'slaving relation' between $\boldsymbol{M}$ and the strain field $\boldsymbol{\epsilon}(\boldsymbol{x},t)$ takes the form of an algebraic system expressing the conditions of chemical balance:

$$\mathbf{k}^b - \mathbf{k}^u(\boldsymbol{\epsilon})\,\boldsymbol{M} = \mathbf{0}, \tag{74}$$

where $\mathbf{k}^b = k^b\mathbf{I}$ is a second order tensor of (strain independent) binding rates and $\mathbf{k}^u(\boldsymbol{\epsilon})$ is a second order tensor of (strain dependent) unbinding rates. We assume a generalized Bell-form for the tensorial unbinding rate:

$$\mathbf{k}^u(\boldsymbol{\epsilon}) = k^u(\mathbf{I} + e^{\mathbb{K}\boldsymbol{\epsilon}}), \tag{75}$$

where $\mathbb{K}$ is a fourth order tensor encoding the degree of strain dependence of the unbinding kinetics and $k^u > 0$ is a constant. This leads to the following tensorial stress-strain relation

$$\boldsymbol{\sigma} = \mathbb{C}^e\epsilon + \mathbb{A}\boldsymbol{M} = \mathbb{C}^e\epsilon + \mathbb{A}(\mathbf{k}^u(\boldsymbol{\epsilon}))^{-1}\mathbf{k}^b\,. \tag{76}$$

The corresponding linearized response is characterized by the active prestress

$$\boldsymbol{\sigma}_{pre} = (k^b/2k^u)\mathbb{A}\mathbf{I},$$

and the actively renormalized linear elastic stiffness tensor

$$\mathbb{C} = \mathbb{C}^e - (k^b/4k^u)\mathbb{A}\hat{\mathbb{K}}.$$

The remaining terms in (76) describes the activity-induced nonlinear (quasi)elasticity.

5.3. 2D isotropic solid

To visualize the emergence of new active energy minima, as the system crosses the *elastic spinodal* thresholds, we now consider in detail the 2D isotropic case. Using a polynomial approximation of the exponential in (75) up to cubic order of strain we can present the associated effective elastic energy density in the form of a Landau-type quartic expansion

$$\begin{aligned} w(\boldsymbol{\epsilon}) \;&=\; (B/2)\epsilon_{mm}\epsilon_{nn} + \mu\,\tilde{\epsilon}_{mn}\tilde{\epsilon}_{mn} \\ &+\; (B'/4)\epsilon_{mm}\epsilon_{nn}\epsilon_{pp}\epsilon_{qq} + \mu'\,\tilde{\epsilon}_{mn}\tilde{\epsilon}_{mn}\tilde{\epsilon}_{pq}\tilde{\epsilon}_{pq}. \end{aligned} \tag{77}$$

where the linearized strain

$$\epsilon_{mn} := (\partial_n u_m + \partial_m u_n)/2 \tag{78}$$

plays the role of a tensorial order parameter. In (77) we used the standard tensorial notations: ϵ_{mm} (summation is assumed over repeated indices) is the trace while $\tilde{\epsilon}_{mn} = \epsilon_{mn} - (\epsilon_{kk})/2\delta_{mn}$ is the deviatoric part of ϵ_{mn}. Note we have included in (77), both the activity renormalized linear elastic moduli B and μ and the the activity induced third order moduli $B' > 0$ and $\mu' > 0$. We have for convenience ignored the cubic terms in (77), including a dilation-shear coupling, because the analysis shows that it has no effect on the discussion of *elastic spinodals*.

In terms of principal strains the expression (77) can be rewritten as follows

$$w(\boldsymbol{\epsilon}) = \frac{B}{2}(\epsilon_1+\epsilon_2)^2+\frac{\mu}{2}(\epsilon_1-\epsilon_2)^2+\frac{B'}{4}(\epsilon_1+\epsilon_2)^4+\frac{\mu'}{4}(\epsilon_1-\epsilon_2)^4. \tag{79}$$

While using the energy density formulation in the scalar case is well justified, in the tensorial case, the assumption that there exists a single scalar function such that $w(\boldsymbol{\epsilon}) = \int \boldsymbol{\sigma}\cdot d\boldsymbol{\epsilon}$ effectively underplays the possibility that activity disrupts the variational structure of the model producing non-reciprocal mechanical interactions. A detailed analysis of an interplay between the corresponding 'odd' effects [95] and the *elastic spinodals* is left for a separate study.

Assuming as before that

$$\hat{\mathbb{K}}_{ijkl} = \hat{K}_b\,\delta_{ij}\delta_{kl} + \hat{K}_s(\delta_{ik}\delta_{jl}+\delta_{il}\delta_{jk}) \tag{80}$$

we can express the effective isotropic elastic moduli in the form

$$B = B^e - (\zeta k^b/k^u)K_b, \tag{81}$$

$$\mu = \mu^e - (\xi k^b/k^u)\hat{K}_s, \tag{82}$$

where, again,

$$B^e = \lambda^e + \mu^e \tag{83}$$

and

$$K_b = \hat{K}_b + 2\Big(1+\frac{\xi}{\zeta}\Big)\hat{K}_s. \tag{84}$$

To obtain the explicit expressions for the third order effective moduli B' and μ', we ignore the dilation-shear couplings as mentioned before, and write the cubic term in the small strain expansion for stress in the form

$$2(\zeta+\xi)\hat{K}_b^3\,\epsilon^3\,\mathbf{I} + 8\zeta\,\hat{K}_s^3\,(\mathrm{tr}\,\boldsymbol{\epsilon}^3)\,\mathbf{I} + 16\xi\,\hat{K}_s^3\,\boldsymbol{\epsilon}^3. \tag{85}$$

From (85) we obtain

$$B' = (k^b/24k^u)(\zeta+\xi)\hat{K}_b^3 \tag{86}$$

and

$$\mu' = (k^b/12k^u)\xi\,\hat{K}_s^3. \tag{87}$$

5.3.1. *Thermodynamic spinodals*

To locate the thermodynamic spinodals we need to determine the configurations where the effective elastic energy (77) loses convexity. Consider an arbitrary local state with a strain $\boldsymbol{\epsilon} = \|\epsilon_{mn}\|$ and introduce a small affine strain perturbation characterized by the second order symmetric tensor $\mathbf{A} = \|a_{ij}\|$. The requirement for the tangential stiffness tensor to be positive definite, ensuring the convexity of the elastic energy, can be formulated in terms of the eigenvalues of the corresponding quadratic form

$$\begin{aligned}\mathbb{C}\mathbf{A}\cdot\mathbf{A} \;=\; & B\,(\mathrm{tr}\,\mathbf{A})^2 + \mu\Big(2|\mathbf{A}|^2 - (\mathrm{tr}\,\mathbf{A})^2\Big)\\ & +3B'\,(\mathrm{tr}\,\boldsymbol{\epsilon})^2(\mathrm{tr}\,\mathbf{A})^2\\ & +2\mu'\,|\tilde{\boldsymbol{\epsilon}}|^2\Big(2|\mathbf{A}|^2 - (\mathrm{tr}\,\mathbf{A})^2\Big) + 8\mu'\,(\tilde{\boldsymbol{\epsilon}}\cdot\mathbf{A})^2\,.\end{aligned} \tag{88}$$

Here $\mathbb{C} = \|C_{ijkl}\|$ is the strain dependent stiffness tensor with components

$$\begin{aligned}&C_{ijkl}(\boldsymbol{\epsilon}) = \partial^2 w/\partial\epsilon_{ij}\,\partial\epsilon_{kl} =\\ &B\,\delta_{ij}\delta_{kl} + \mu\,(\delta_{ik}\delta_{jl}+\delta_{il}\delta_{jk}-\delta_{ij}\delta_{kl}) + 3B'\,(\epsilon_{mm})^2\delta_{ij}\delta_{kl}\\ &+2\mu'\,\tilde{\epsilon}_{pq}\tilde{\epsilon}_{pq}(\delta_{ik}\delta_{jl}+\delta_{il}\delta_{jk}-\delta_{ij}\delta_{kl}) + 8\mu'\,\tilde{\epsilon}_{ij}\tilde{\epsilon}_{kl}.\end{aligned} \tag{89}$$

Choosing $\mathbf{A}$ to be a dilation, $\mathbf{A} = A\,\mathbf{I}$, we obtain

$$\mathbb{C}\mathbf{A}\cdot\mathbf{A} = 16\Big(B + 3B'\,(\epsilon_1+\epsilon_2)^2\Big)A^2, \tag{90}$$

where $\epsilon_{1,2}$ are again the principal strains. This gives one condition defining thermodynamic spinodal

$$B + 3B'\,(\epsilon_1+\epsilon_2)^2 = 0. \tag{91}$$

If instead we choose $\mathbf{A}$ to be deviatoric, we get

$$\begin{aligned}0 \le \mathbb{C}\mathbf{A}\cdot\mathbf{A} &= \\ 2\mu\,|\mathbf{A}|^2 + 4\mu'\,|\tilde{\boldsymbol{\epsilon}}|^2|\mathbf{A}|^2 + 8\mu'\,(\tilde{\boldsymbol{\epsilon}}\cdot\mathbf{A})^2 &\\ \le 2\Big(\mu + 6\mu'\,|\tilde{\boldsymbol{\epsilon}}|^2\Big)|\mathbf{A}|^2 &\\ \le 2\Big(\mu + 3\mu'\,(\epsilon_1-\epsilon_2)^2\Big)|\mathbf{A}|^2,\end{aligned} \tag{92}$$

where we used the Cauchy-Schwarz inequality $(\tilde{\boldsymbol{\epsilon}}\cdot\mathbf{A})^2 \le |\tilde{\boldsymbol{\epsilon}}|^2|\mathbf{A}|^2$ to obtain the upper bound. If the right hand sides of (92) vanishes, the corresponding strain state $\boldsymbol{\epsilon}$ lies on the thermodynamic spinodal and therefore we obtain the second condition

$$\mu + 3\mu'\,(\epsilon_1-\epsilon_2)^2 = 0. \tag{93}$$

given that dilational and deviatoric deformations form orthogonal basis in the space of symmetric tensors which diagonalizes our quadratic form, we can conclude that the two (strain dependent) equations (91) and (93) fully characterize the thermodynamic spinodal in the model of 2D isotropic nonlinear elasticity (77).

5.3.2. Elastic spinodals

We recall that *elastic spinodals* delineate the region in the strain space $\boldsymbol{\epsilon}$ where the strain-dependent acoustic tensor $\mathbf{Q}(\mathbf{q})$ remains positive definite. In other words, at an *elastic spinodal*, at least one eigenvalue of this tensor vanishes.

In the material model (77) the expression for the (strain dependent) acoustic tensor takes the form

$$\begin{aligned} Q_{ik}(\mathbf{q}) &= C_{ijkl} q_j q_l \\ &= B\, q_i q_k + \mu\, \delta_{ik} + 3B'\,(\epsilon_{mm})^2\, q_i q_k \\ &\quad + 2\mu'\,|\tilde{\boldsymbol{\epsilon}}|^2\, \delta_{ik} + 8\mu'\,\tilde{\epsilon}_{ij} q_j\, \tilde{\epsilon}_{kl} q_l . \end{aligned} \tag{94}$$

As in (36), we can use here the orthonormal basis $(\mathbf{q}\otimes\mathbf{q},\ \mathbf{q}_\perp\otimes\mathbf{q}_\perp)$, formed by the Fourier space wave vector $\mathbf{q}$ and its orthogonal complement $\mathbf{q}_\perp$, to rewrite the above expression in the form

$$\begin{aligned} &\mathbf{Q}(\mathbf{q}) = \\ &\Big(B + 3B'\,(\operatorname{tr}\boldsymbol{\epsilon})^2 + \mu + 2\mu'\,|\tilde{\boldsymbol{\epsilon}}|^2 + 8\mu'\,(\tilde{\boldsymbol{\epsilon}}\mathbf{q}\cdot\mathbf{q})^2\Big)\mathbf{q}\otimes\mathbf{q} \\ &+\Big(\mu + 2\mu'\,|\tilde{\boldsymbol{\epsilon}}|^2 + 8\mu'\,(\tilde{\boldsymbol{\epsilon}}\mathbf{q}\cdot\mathbf{q}_\perp)^2\Big)\mathbf{q}_\perp\otimes\mathbf{q}_\perp . \end{aligned} \tag{95}$$

From this orthogonal representation one can see that vanishing of the eigenvalue associated with the longitudinal modes $\mathbf{q}\otimes\mathbf{q}$ gives one branch of the *elastic spinodal*

$$B + 3B'\,(\operatorname{tr}\boldsymbol{\epsilon})^2 + \mu + 2\mu'\,|\tilde{\boldsymbol{\epsilon}}|^2 + 8\mu'\,(\tilde{\boldsymbol{\epsilon}}\mathbf{q}\cdot\mathbf{q})^2 = 0\,, \tag{96}$$

which under linearization (96) converges to the elastic aether threshold. Similarly, vanishing of the eigenvalue associated with the transverse/shear modes $\mathbf{q}_\perp\otimes\mathbf{q}_\perp$ gives the other branch of the *elastic spinodal*

$$\mu + 2\mu'\,|\tilde{\boldsymbol{\epsilon}}|^2 + 8\mu'\,(\tilde{\boldsymbol{\epsilon}}\mathbf{q}\cdot\mathbf{q}_\perp)^2 = 0. \tag{97}$$

Expectedly, under linearization (97) converges to the elastic liquid threshold. If we now diagonalize the strain tensor using the basis $\boldsymbol{\epsilon} = \epsilon_1\,\mathbf{q}\otimes\mathbf{q} + \epsilon_2\,\mathbf{q}_\perp\otimes\mathbf{q}_\perp$, Eqs. (96) and (97) reduce, respectively, to the following equations defining the segments of the *elastic spinodal* in the space of principal strains:

$$B + \mu + 3B'(\epsilon_1+\epsilon_2)^2 + 3\mu'\,(\epsilon_1-\epsilon_2)^2 = 0, \tag{98a}$$

$$\mu + \mu'\,(\epsilon_1-\epsilon_2)^2 = 0. \tag{98b}$$

From the expressions of the effective parameters B, μ, B' and μ', given in (81)-(87), we observe that if B^e, $\mu^e > 0$, and the system exhibits 'catch bond' type kinetics ($\hat{K}_{b,s} > 0$), increasing activity levels ζ, $\xi > 0$ can drive the effective linear elastic moduli B and μ to change the sign and become negative, while the nonlinear elastic moduli remain positive (B', $\mu' > 0$). In other words, activity alone can induce the emergence of *elastic spinodals*.

5.3.3. Active remodelling of the energy landscape

As the activity levels $\xi > 0$ and $\zeta > 0$ change, the energy landscapes (77, 79) evolve. In Fig. 7 we trace the modifications in the location of the nonlinear *elastic spinodals* in the space of principal strains as the system crosses the 'naive' *elastic spinodal* thresholds $\mu = 0$ and $B + \mu = 0$ of the linearized model. While the latter are derived from a linearized analysis of the elastic energy around the reference state, the 'true' *elastic spinodals* are generically reached at a nonzero level of strain.

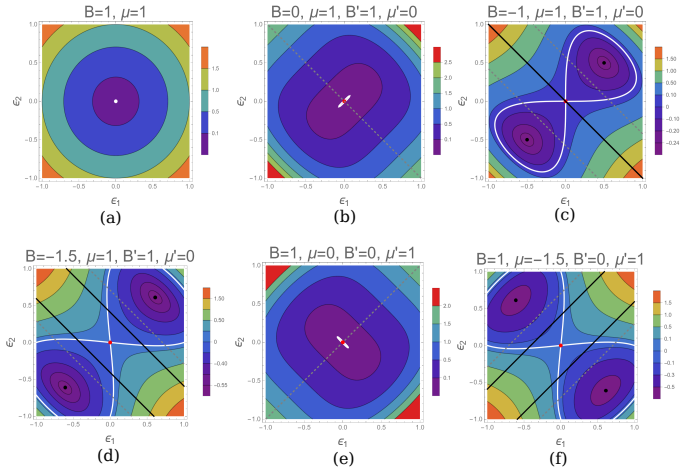

FIG. 7. Evolution of the effective energy landscape $w(\epsilon_1, \epsilon_2)$ as activities ζ, ξ increase, leading to the appearance of new energy minima; (a) passive solid; active solid at (b) the thermodynamic spinodal, (c) aether, (d) post-aether, (e) elastic liquid, and (f) elastic post-liquid regime. In (b-f), elastic and thermodynamic spinodals are shown by solid and dotted lines, respectively. White lines mark zero energy valleys.

Note that in the nonlinear regime, the 'naive' thresholds $\mu = 0$ or $B + \mu = 0$ mark the points of activity-induced second order phase transitions (critical points). Specifically, when the elastic liquid threshold $\mu = 0$ is crosses at the activity level $\xi = -\mu^e/(2K_s)$, the two new energy minima emerge along the shear axis, $\epsilon_1 - \epsilon_2$, while along the perpendicular hydrostatic axis $\epsilon_1 + \epsilon_2$ the energy remains convex, see Fig. 7. Similarly, passing the elastic aether threshold $B + \mu = 0$ at the activity level $\zeta = -(B^e + \mu^e)/2K_b$ generates two new minima along the hydrostatic axis $\epsilon_1 + \epsilon_2$ while along the perpendicular shear axis $\epsilon_1 - \epsilon_2$ the convexity of the energy is preserved. Note also that in the post-liquid regimes with $\mu \lesssim 0$, the two emerging active energy minima, shown in Fig. 7, are in fact connected and are, therefore, degenerate, as they represent a continuous family of pure shears related through rigid rotations. The corresponding energy minimizing mixtures should resemble microstructures encountered in nematic elastomers [189]; under some additional assumptions, a pronounced force channeling has been observed numerically in such nonlinear elastic models [61, 190]. Instead, in the post-aether

regimes with $B \lesssim -\mu$, the emerging active nonlinear energy minima, shown in Fig. 7, are isolated and represent configurations with different densities. The energy minimizing microstructures in such nonlinear elastic materials with purely volumetric phase transitions are simple laminates unless the shear modulus μ is extremely small [191, 192].

The *elastic spinodals* of the nonlinear system (black lines in Fig. 7) can also be reached by external mechanical loading [193]. In the cellular context, this can be achieved by subjecting the body to external forces, say through embedded magnetic beads, by using optical tweezers [12], or by deforming the substrate [51]. External loading can be also be achieved by the presence of the surrounding cells in a confluent tissue [103]. The same marginal responses can be also realized in the cellular context actively [194–200], for instance, through internal force transducers such as myosin or focal adhesions [18, 22, 107]. We further observe that, as in linear case, the thermodynamic spinodals of the nonliner model (gray dotted lines in Fig. 7), lie 'inside' the elastic spinodals (if one advances from the stable domain).

5.3.4. *Force channeling*

We now demonstrate the phenomenon of stress channeling in the active material with a (quasi)elastic response governed by (77). To this end, we choose a slightly post-aether regime characterized by the dimensionless parameters: $B = -1.02$, $\mu = 1$, $B' = 1$, $\mu' = 0.005$, see Fig. 8(b). In this near-critical state, the reference configuration is unstable, and the *elastic spinodal* bounds a spinodal region dominated by small-strain pure shear states $\epsilon_1 + \epsilon_2 \approx 0$. Such unstable states can be expected to decompose into a mixture of two active energy wells, corresponding to high- and low-density configurations. In the resulting microstructures the force channeling will then occur along 'chain' structures composed of the denser material.

To 'round' the emerging singularities and control stress concentration, we need to regularize the scale-free model (77), which will also eliminate mesh dependence in our numerical simulation. This is achieved by adding a strain gradient term to the energy density, transforming the Landau-type potential $w(\boldsymbol{\epsilon})$ into a Ginzburg-Landau-type form:

$$w(\boldsymbol{\epsilon}, \nabla\boldsymbol{\epsilon}) = w(\boldsymbol{\epsilon}) + (\kappa/2)|\nabla\boldsymbol{\epsilon}|^2. \tag{99}$$

Here, the parameter κ introduces an internal length scale into the model, capturing the degree of nonlocal effects. To minimize interference of this nonlocality with the formation of microstructure, we chose κ to be sufficiently small, $\kappa = 0.0001$. With the regularized energy density (99), where the function $w(\boldsymbol{\epsilon})$ is taken from (77), the expression of stress acquires a higher strain gradient

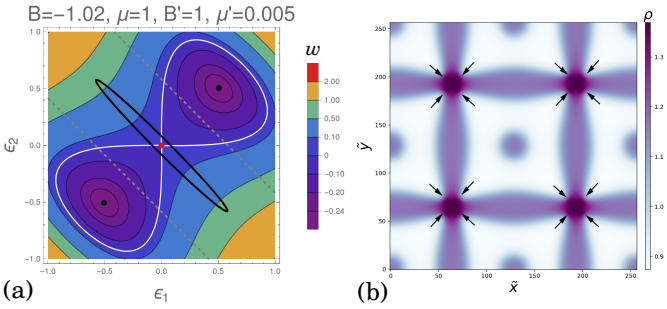

FIG. 8. (a) Contour plot of the effective energy landscape in the space of principal strains $w(\epsilon_1, \epsilon_2)$ in a weakly post-aether regime $B = -1.02$, $\mu = 1$, $B' = 1$, $\mu' = 0.005$. Strain localization in such post-aether regime is illustrated in (b), where ρ is the density of the material, represented in the deformed coordinates.

correction

$$\boldsymbol{\sigma}(\boldsymbol{\epsilon}) = \Big[B\,\mathrm{tr}\,\boldsymbol{\epsilon} + B'(\mathrm{tr}\,\boldsymbol{\epsilon})^3\Big]\mathbf{I} + 2\mu\tilde{\boldsymbol{\epsilon}} + \mu'\tilde{\boldsymbol{\epsilon}}^3 - \kappa\nabla^2\boldsymbol{\epsilon}. \tag{100}$$

We used (100) in an overdamped model

$$\Gamma\frac{\partial \boldsymbol{u}}{\partial t} = \mathrm{div}\,\boldsymbol{\sigma} + \mathbf{f}, \tag{101}$$

where $\mathbf{f}(\boldsymbol{x})$ is an applied force field and Γ is the environmental viscosity coefficient. In our numerical simulations we used dimesnionless variables normilizing length with $(\kappa/\mu)^{-1/2}$, and time with $\Gamma^{-1}(\kappa/\mu)^{-3/2}$.

Solving (101) ensures local energy minimization at each increment of quasi-static loading. The nature of dynamics changes only when the system reaches the end of a continuous branch of elastic equilibria. In such points the equation (101) describes fast (at the time scale of the loading) mechanical relaxation towards the closest local energy minimum.

The system (101) was integrated numerically in a 2D square domain with periodic boundary conditions, which allowed us to use a spectral method [201]. To mimic endogenous body forces we considered the local loading $\mathbf{f} = \sum_{\alpha=1}^{4}\mathbf{f}^{(\alpha)}$ representing two perpendicular contractile force dipoles mimicking a center of active contraction. In view of periodicity of the boundary conditions we effectively introduced a periodic lattice of quadrupoles, see Fig. 8(b).

As initial conditions we chose a homogeneous initial state representing an unstable reference configuration located inside the narrow spinodal region, Fig. 8(a). A intermediate outcome of the ensuing process of elastic spinodal decomposition is illustrated in Fig. 8(b) where we show the computed defomred density distribution

$$\rho(\boldsymbol{x}) = \Big(\det\left(\mathbf{I} + \nabla\boldsymbol{u}\right)\Big)^{-1}; \tag{102}$$

here, we have implicitly assumed that the uniform density of the reference material is 1. For better clarity, ρ is

presented in the coordinates of the deformed configuration

$$\bar{\boldsymbol{x}} = \boldsymbol{x} + \boldsymbol{u}(\boldsymbol{x}). \tag{103}$$

The corresponding time evolution can be seen in a movie available at SMOV where we also visualize the dynamics of dilational $\mathrm{tr}\,\boldsymbol{\sigma}$ and deviatoric $|\tilde{\boldsymbol{\sigma}}|$ stress measures.

The density localizations connecting contractile centers in Fig. 8(b) and the corresponding depletion outside these regions can be interpreted as the formation of a force-chain pattern. Given that our model presents only a minimal prototypical framework, we do not attempt here a detailed comparison with such patterns observed experimentally [66, 202, 203].

Specifically, a more comprehensive, experimentally calibrated model describe the mechanical properties of active actomyosin cytoskeleton should be tested against observations on cells adhered to micro-patterned substrates [51], confluent tissues [31], and in vitro reconstituted systems with controlled mechanical constraints [204]. To be realistic, such model should account for the fact that in such active material the access to elastically degenerate regimes may arise from micromechanical phenomena such as microbuckling [16], crosslinker loss leading to filament sliding [73], micro-wrinkling [74], and stretching-to-bending transitions [75–79]. Capturing these mechanisms requires microscopic modeling, incorporating the dynamic assembly and disassembly of the cytoskeletal elements. This would allow, for instance, for the description of the observed transient stress fiber formation and their potential merging into force-carrying frames [12].

6. MICROSCOPIC STOCHASTIC MODEL

So far, the nonequilibrium nature of the drive towards elastic spinodals was concealed behind the assumption that active stresses could be represented by an effective (quasi)elastic energy density. To address the out of equilibrium aspects of the emerging (quasi)elastic behavior we consider here the simplest zero dimensional model. The goal here is to illustrate the idea that behind the implied 'renormalization' of the elastic energy there is a continuous energy exchange with a non-equilibrium energy reservoir. The analysis below can be viewed as an elaboration of the model proposed in [28]; for other related developments see [29, 30, 40].

Consider an overdamped ratchet-type stochastic system described by the Langevin equation and schematically illustrated in the inset in Fig. 9(a)

$$\dot{x} = -\partial_x G + \sqrt{2D}\eta(t). \tag{104}$$

Here $\eta(t)$ is a standard white noise with unit variance, D is a measure of temperature and

$$G(x,t) = V(x) - xf(t) + k(x-z)^2/2 \tag{105}$$

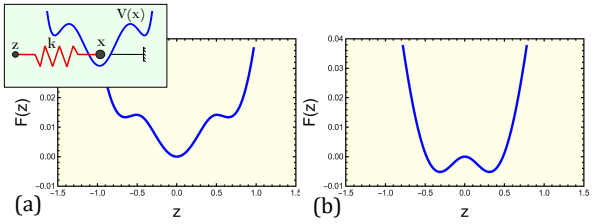

FIG. 9. The effective potential $F(z)$ at different levels of activity: (a) $A = 0$ and (b) $A = 0.4$, with $D = 0.01$.

where

$$V(x) = (1/2)(x^2 - 0.1)(x^2 - 0.5)^2 \tag{106}$$

is a polynomial Landau-type elastic energy (non-renormalized) and $f(t)$ is a time correlated rocking force with zero average. Note that we have also implicitly assumed that the configuration of this non-equilibrium system is continuously probed through a spring with stiffness k. In this case the variable z plays the role of an external control parameter, see the inset in Fig. 9(a).

The effective force exerted on the spring and recorded by the external loading device can be found by averaging the response $x(t)$ over ensemble and over time, which gives

$$T(z) = k[z - \lim_{t\to\infty}(1/t)\int_0^t \int_{-\infty}^{\infty} xp(x,t')dxdt']. \tag{107}$$

To find the probability distribution $p(x,t)$ one must find the corresponding time dependent solution of the Fokker-Planck equation

$$\partial_t p = \partial_x \left[p\partial_x G + D\partial_x p\right]. \tag{108}$$

After the function $T(z)$ is known, one can determine the non-equilibrium (quasi)elastic energy simply by integration

$$F(z) = \int^z T(s)ds. \tag{109}$$

The function $F(z)$ would then play the role of an active renormalization of the original passive elastic energy.

Suppose further that the correlated driving signal $f(t)$ is periodic and or analytical simplicity choose it the simplest piece-wise constant form

$$f(t) = A(-1)^{n(t)}, \tag{110}$$

where $n(t) = \lfloor 2t/\tau \rfloor$. The advantage of this choice is that the ensuing mathematical problem can be solved analytically in the adiabatic approximation, see [205] for a similar analysis.

To develop such an approximation, we assume that the time scale τ is large comparing to the time scale of the thermally induced barrier crossing in the original potential $V(x)$. We can then focus on the time intervals where the driving force is constant

$$f(t) \equiv A. \tag{111}$$

The solution of the corresponding time-independent Fokker-Planck equation

$$\partial_x \left[p\partial_x G + D\partial_x p\right] = 0 \tag{112}$$

can be written explicitly

$$p_A(x) = Z^{-1} e^{-G(x,z)/D}, \tag{113}$$

where we introduced the normalization constant

$$Z = \int_{-\infty}^{\infty} e^{-G(x,z)/D} dx. \tag{114}$$

Given our assumption of time scale separation, we can now write the time-averaged probability distribution in the form

$$p_{\rm ad}(x) = (p_A(x) + p_{-A}(x))/2. \tag{115}$$

Our results are illustrated in Fig. 9(a,b) where we show the evolution of the elastic energy of the system as the level of activity measured by the rocking amplitude A changes from zero, $A = 0$, to a finite value $A > 0$. Note that the energy minimum at $z = 0$ which corresponds to stable equilibrium in the passive system is transformed by activity into an unstable state representing a local energy maximum. More specifically, under the growing activity level (increasing A), the energy minimum at $z = 0$ first flattens at a critical value $A = A_c$, which marks the state of zero rigidity, and then disappears signaling a second order phase transition. The subsequent growth of activity level reconfigures the energy landscape further favoring two symmetric actively-supported ground states.

While the proposed model is obviously oversimplistic, it shows the possibility of active modification of energy landscapes due to exposure of mechanical systems to nonequilibrium reservoirs. The model can be made more comprehensive if we consider a network of such active springs while representing activity not only through correlated noise but also through hysteretic delays and non-reciprocity [206]. The resulting model would serve as a microscopic description behind the emerging fragility at the coarse grained continuum scale.

7. CONCLUSIONS

In this paper we investigated mechanisms of rigidity loss in isotropic elastic solids and explored how active materials can be directed toward marginal and fragile regimes. A key contribution of this work is refining in the active matter context of the concept of *elastic spinodals*, while stressing their fundamental difference from the more conventional thermodynamic spinodals. While the emergence of degenerate acoustic modes at finite wave numbers has been explored before [94, 95], the active realization of materials where such modes can become mechanically operative has been underplayed. It has been also overlooked that at *elastic spinodal* thresholds, inhomogeneous soft modes not only soften the overall rigidity but also shift the modality of stress propagation from diffusion-like to force channeling.

Unlike thermodynamic spinodals, *elastic spinodals* emerge due to the long-range interactions inherent in elastic systems, where strain — serving as the order parameter — has a gradient structure. In nonlinear elasticity, such states describe minimally stable, marginal deformation gradients. While the conventional engineering designs prioritize instead maximally stable equilibria, there is a growing evidence that biological systems operate near marginal stability which allows them to exploit a repository of zero energy modes. Moreover, as we show, active systems can self-tune towards such states and then exploit them for functional advantage.

Limiting attention only to the simplest case of elastic marginality in isotropic solids, we were able to explore the explicit mechanisms of actively reaching the mechanical regimes with partial rigidity loss. The most striking manifestation of such regimes is stress localization, leading to force channeling along transient low-dimensional substructures, such as stress tethers and force chains. Our key conjecture is that in the presence of nonlinear adaptive feedback mechanisms these structures can be actively assembled and disassembled. In particular, we argued that cellular cytoskeleton exemplifies an active material which is self-tuned towards marginal regime where it dynamically balances solidity and fluidity.

Our study suggests that artificial active materials, equipped with appropriate feedback control mechanisms, can be designed to operate at marginal stability, leveraging complex non-affine soft modes. While such behavior is absent in passive materials, the potential for extreme mechanical responses could inspire bio-mimetic implementations using existing metamaterial approaches [90, 207–214]. On the theoretical front, extending these results to anisotropic [187, 215, 216] and non-reciprocal (odd) elastic materials [95] would likely reveal new fragile soft modes and spinodal regimes. Additionally, future studies should investigate fragility in active solids with elastic incompatibility, where activity may drive defect proliferation and quasi-plastic behavior [217].

8. ACKNOWLEDGMENTS

The authors thank A. Gupta and G. Zurlo for helpful discussions. AR and MR acknowledge support from the Department of Atomic Energy (India), under project no. RTI4006, and the Simons Foundation (Grant No. 287975), and computational facilities at NCBS. MR acknowledges a JC Bose Fellowship from DST-SERB (India). LT was supported by the grants ANR-17-CE08-0047-02, ANR–21-CE08-MESOCRYSP and ERC-H2020-MSCA-RISE-2020-101008140.

[1] P. M. Chaikin and T. C. Lubensky, *Principles of Condensed Matter Physics*, Cambridge University Press (1995).

[2] J. C. Maxwell, *On the calculation of the equilibrium and stiffness of frames*, Philosophical Magazine **27**, 294 (1864).

[3] A. J. Liu and S. R. Nagel, *Jamming is not cool anymore*, Nature **396**, 21 (1998).

[4] S. F. Edwards and D. V. Grinev, *Statistical Mechanics of Stress Transmission in Disordered Granular Arrays*, Physical Review Letters **82**, 5397 (1999).

[5] W. G. Ellenbroek, Z. Zeravcic, W. van Saarloos and M. van Hecke, *Non-affine response: Jammed packings vs. spring networks*, Europhysics Letters **87**, 34004 (2009).

[6] P. R. Onck, T. Koeman, T. van Dillen and E. van der Giessen, *Alternative Explanation of Stiffening in Cross-Linked Semiflexible Networks*, Physical Review Letters **95**, 178102 (2005).

[7] S. Alexander, *Amorphous solids: Their structure, lattice dynamics and elasticity*, Physics Reports **296**, 65–236 (1998).

[8] C. R. Calladine, *Buckminster Fuller's "Tensegrity" structures and Clerk Maxwell's rules for the construction of stiff frames*, International Journal of Solids and Structures **14**, 161–172 (1978).

[9] M. Merkel, K. Baumgarten, B. P. Tighe, and M. L. Manning, *A minimal-length approach unifies rigidity in underconstrained materials*, Proceedings of the National Academy of Sciences **116**, 6560-6568 (2019).

[10] C-T. Lee and M. Merkel, *Stiffening of under-constrained spring networks under isotropic strain*, Soft Matter **18**, 5410 (2022).

[11] X. Mao and T. C. Lubensky, *Maxwell Lattices and Topological Mechanics*, Annual Review of Condensed Matter Physics **9**, 413-433 (2018).

[12] D. E. Ingber, N. Wang and D. Stamenović, *Tensegrity, cellular biophysics, and the mechanics of living systems*, Reports on Progress in Physics **77**, 046603 (2014).

[13] B. I. Halperin and D. R. Nelson, *Theory of two-dimensional melting*, Physical Review Letters **41**, 121–124 (1978).

[14] C. P. Goodrich, A. J. Liu and S. R. Nagel, *The Principle of Independent Bond-Level Response: Tuning by Pruning to Exploit Disorder for Global Behavior*, Physical Review Letters **114**, 225501 (2015).

[15] M. E. Cates, J. P. Wittmer, J. -P. Bouchaud and P. Claudin, *Jamming, force chains, and fragile matter*, Physical Review Letters **81**, 1841–1844 (1998).

[16] P. Ronceray, C. P. Boedersz and M. Lenz, *Fiber networks amplify active stress*, Proceedings of the National Academy of Sciences **113**, 2827–2832 (2016).

[17] R. H. Pritchard, Y. Y. S. Huang and E. M. Terentjev, *Mechanics of biological networks: from the cell cytoskeleton to connective tissue*, Soft Matter **10**, 1864–1884 (2014).

[18] D. Humphrey, C. Duggan, D. Saha, D. Smith and J. Käs, *Active fluidization of polymer networks through molecular motors*, Nature **416** (6879), 413-416 (2002).

[19] W. Xi, T. B. Saw, D. Delacour, C. T. Lim and B. Ladoux, *Material approaches to active tissue mechanics*, Nature Reviews Materials **4**, 23-44 (2019).

[20] H. Schillers, M. Wälte, K. Urbanova and H. Oberleithner, *Real-Time Monitoring of Cell Elasticity Reveals Oscillating Myosin Activity*, Biophysical Journal **99**, 3639–3646 (2010).

[21] J. Étienne, J. Fouchard, D. Mitrossilis, N. Bufi, P. Durand-Smet and A. Asnacios, *Cells as liquid motors: Mechanosensitivity emerges from collective dynamics of actomyosin cortex*, Proceedings of the National Academy of Sciences **112**, 2740–2745 (2015).

[22] G. H. Koenderink, Z. Dogic F. Nakamura, P. M. Bendix, F. C. MacKintosh, J. H. Hartwig, T. P. Stossel and D. A. Weitz, *An active biopolymer network controlled by molecular motors*, Proceedings of the National Academy of Sciences **106**, 15192–15197 (2009).

[23] R. J. Hawkins and T. B. Liverpool, *Stress Reorganisation and Response in Active Solids*, Physical Review Letters **113**, 028102 (2014).

[24] T. Hiraiwa and G. Salbreux, *Role of Turnover in Active Stress Generation in a Filament Network*, Physical Review Letters **116**, 188101 (2016).

[25] K. L. Weirich, S. Banerjee, K. Dasbiswas, T. A. Witten, S. Vaikuntanathan and M. L. Gardel, *Liquid behavior of cross-linked actin bundles*, Proceedings of the National Academy of Sciences **114**, 2131-2136 (2017).

[26] K. L. Weirich, S. Stam, E. Munro and M. L. Gardel, *Actin bundle architecture and mechanics regulate myosin II force generation*, Biophysical Journal **120**, 1957-1970 (2021).

[27] D. Oriola, R. Alert and J. Casademunt, *Fluidization and active thinning by molecular kinetics in active gels*, Physical Review Lettrs **118**, 088002 (2017).

[28] R. Sheshka, P. Recho and L. Truskinovsky, *Rigidity generation by nonthermal fluctuations*, Physical Review E **93**, 052604 (2016).

[29] A. Maitra and R. Voituriez, *Enhanced Orientational Ordering Induced by an Active yet Isotropic Bath*, Physical Review Letters **124**, 048003 (2020).

[30] A. Behera, M. Rao, S. Sastry and S. Vaikuntanathan, *Enhanced Associative Memory, Classification, and Learning with Active Dynamics*, Physical Review X **13**, 041043 (2023).

[31] D. S. Banerjee, A. Munjal, T. Lecuit and M. Rao, *Actomyosin pulsation and flows in an active elastomer with turnover and network remodeling*, Nature Communications **8**, 1121 (2017).

[32] A. Roychowdhury, S. Dasgupta and M. Rao, *Emergence of Tension Chains and Active Force Patterning*, arXiv:2206.06770 (2022).

[33] J.-P. Bouchaud, P. Claudin, M.E. Cates, J.P. Wittmer, *Models of stress propagation in granular media*, in Physics of Dry Granular Media, H.J. Herrmann, J.P. Hovi and S. Luding (Eds.), NATO ASI, 97–121 (1997).

[34] S. Ramaswamy and M. Rao, *Active-filament hydrodynamics: instabilities, boundary conditions and rheology*, New Journal of Physics **9**, 423 (2007).

[35] M. E. Cates and M. R. Evans (Eds.), *Soft and fragile matter: nonequilibrium dynamics, metastability and flow* (PBK), CRC Press (2000).

[36] V. Vitelli and M. van Hecke, *Shocks in fragile matter*, Europhysics News **43**, 36-39 (2012).

[37] D. Pan, Y. Wang, H. Yoshino, J. Zhang and Y. Jin, *A review on shear jamming*, arXiv preprint arXiv:2306.13416 (2023).

[38] V. Vitelli and M. van Hecke, *Marginal matters*, Nature **480**, 325-326 (2011).

[39] T. C. Lubensky, C. L. Kane, X. Mao, A. Souslov and K. Sun, *Phonons and elasticity in critically coordinated lattices*, Reports on Progress in Physics **78**, 073901 (2015).

[40] M. M. Driscoll, B. Gin-ge Chen, T. H. Beuman and V. Vitelli, *The role of rigidity in controlling material failure*, Proceedings of the National Academy of Sciences **113**, 10813-10817 (2016).

[41] C. J. Gagne, H. Gould, W. Klein, T. Lookman and A. Saxena, *Simulations of spinodal nucleation in systems with elastic interactions*, Physical Review Letters **95**, 095701 (2005).

[42] W. Klein, T. Lookman, A. Saxena and D. M. Hatch, *Nucleation in systems with elastic forces*, Physical Review Letters **88**, 085701 (2002).

[43] A. O. Schweiger, K. Barros and W. Klein, *Transient nucleation near the mean-field spinodal*, Physical Review E **75**, 031102 (2007).

[44] L. Zhang, D. Z. Rocklin, L. M. Sander and X. Mao, *Fiber networks below the isostatic point: Fracture without stress concentration*, Physical Review Materials **1**, 052602 (2017).

[45] S. F. Edwards, *The equations of stress in a granular material*, Physica A **249**, 226–231 (1998).

[46] T. D. Pollard and R. D. Goldman (Editors), *The Cytoskeleton*, Cold Spring Harbor Laboratory Press (2016).

[47] N. Wang, J. P. Butler and D. E. Ingber, *Mechanotransduction across the cell surface and through the cytoskeleton*, Science **260**, 1124–1127 (1993).

[48] B. D. Matthews, D. R. Overby, R. Mannix and D. E. Ingber, *Cellular adaptation to mechanical stress: role of integrins, Rho, cytoskeletal tension and mechanosensitive ion channels*, Journal of Cell Science **119**, 508–518 (2006).

[49] S. Banerjee, M. L. Gardel and U. S. Schwarz, *The actin cytoskeleton as an active adaptive material*, Annual Review of Condensed Matter Physics **11**, 421–439 (2020).

[50] C. J. Chan, A. E. Ekpenyong, S. Golfier, W. Li, K. J. Chalut, O. Otto, J. Elgeti, J. Guck and F. Lautenschläger, *Myosin II activity softens cells in suspension*, Biophysical Journal **108**, 1856-1869 (2015).

[51] T. Vignaud, C. Copos, C. Leterrier, M. Toro-Nahuelpan, Q. Tseng , J. Mahamid, L. Blanchoin, A. Mogilner, M. Théry and L. Kurzawa, *Stress fibres are embedded in a contractile cortical network*, Nature Materials **20**, 410–420 (2021).

[52] J. I. Lehtimäki, E. K. Rajakylä, S. Tojkander and Pekka Lappalainen, *Generation of stress fibers through myosin-driven re-organization of the actin cortex*, eLife **10**, e60710 (2021).

[53] J. Notbohm, A. Lesman, P. Rosakis, D. A. Tirrell and G. Ravichandran, *Microbuckling in fibrin networks enables long-range cell mechanosensing*, Journal of Royal Society Interface **12**, 20150320 (2015).

[54] T. Nagel and D. J. Kelly, *Remodelling of collagen fibre transition stretch and angular distribution in soft biological tissues and cell-seeded hydrogels*, Biomechanics and Modeling in Mechanobiology **11**, 325–339 (2012).

[55] J. P. Winer, S. Oake and P. A. Janmey, *Nonlinear elasticity of extracellular matrices enables contractile cells to communicate local position and orientation*, PLoS ONE **4**, e6382, doi:10.1371/journal.pone. 0006382, (2009).

[56] H. Wang, A. Abhilash, C.S. Chen, R. G. Wells, and V. B. Shenoy, *Long-range force transmission in fibrous matrices enabled by tension-driven alignment of fibers*, Biophysical Journal **107**, 2592–2603 (2014).

[57] Y. Q. Chen, J. C. Kuo, M. T. Wei, Y. C. Chen, M. H. Yang and A. Chiou, *Early stage mechanical remodeling of collagen surrounding head and neck squamous cell carcinoma spheroids correlates strongly with their invasion capability*, Acta Biomaterialia **84**, 280–292 (2019).

[58] J. Ferruzzi, M. Sun, A. Gkousioudi, A. Pilvar, D. Roblyer, Y. Zhang and M. H. Zaman, *Compressive remodeling alters fluid transport properties of collagen networks—implications for tumor growth*, Scientific Reports **9**, 1–16 (2019).

[59] B. Babaei, A. Davarian, S. L. Lee, K. M. Pryse, W. B. McConnaughey, E. L. Elson and G. M. Genin, *Remodeling by fibroblasts alters the rate- dependent mechanical properties of collagen*, Acta Biomaterialia **37**, 28–37 (2016).

[60] U. Doha, O. Aydin, M. S. H. Joy, B. Emon, W. Drennan and M. T. A. Saif, *Disorder to order transition in cell-ECM systems mediated by cell-cell collective interactions*. Acta Biomaterialia **154**, 290-301 (2022).

[61] G. Grekas, M. Proestaki, P. Rosakis, J. Notbohm, C. Makridakis and G. Ravichandran, *Cells exploit a phase transition to mechanically remodel the fibrous extracellular matrix*. Journal of Royal Society Interface **18** 20200823 (2021).

[62] A. K. Harris, D. Stopak and P. Wild, *Fibroblast traction as a mechanism for collagen morphogenesis*, Nature **290**, 249–251 (1981).

[63] D. Vader, A. Kabla, D. Weitz and L. Mahadevan, *Strain-induced alignment in collagen gels*, PLoS ONE **4**, e5902 (2009).

[64] Q. Shi, R. P. Ghosh, H. Engelke, C. H. Rycroft, L. Cassereau, J. A. Sethian, V. M. Weaver and J. T. Liphardt, *Rapid disorganization of mechanically interacting systems of mammary acini*, Proceedings of National Academy of Sciences **111**, 658–663 (2014).

[65] E. Ban, J. M. Franklin, S. Nam, L. R. Smith, H. Wang, R. G. Wells, O. Chaudhuri, J. T. Liphardt and V. B. Shenoy, *Mechanisms of plastic deformation in collagen networks induced by cellular forces*, Biophysical Journal **114**, 450–461 (2018).

[66] A. Favata, A. Rodella and S. Vidoli, *Emerging anisotropy and tethering with memory effects in fibrous materials*, Mechanics of Materials **190**, 104928 (2024).

[67] N. Wang and Z. Suo, *Long-distance propagation of forces in a cell*, Biochemical and Biophysical Research Communications **328**, 1133–1138 (2005).

[68] D. E. Jaalouk and J. Lammerding, *Mechanotransduction gone awry*, Nature Reviews Molecular Cell Biology **10**, 63–73 (2009).

[69] R. Blumenfeld, *Isostaticity and Controlled Force Transmission in the Cytoskeleton: A Model Awaiting Experimental Evidence*, Biophysical Journal **91**, 1970–1983 (2006).

[70] S. Na, O. Collin, F. Chowdhury, B. Tay, M. Ouyang, Y. Wang and N. Wang, *Rapid signal transduction in living cells is a unique feature of mechanotransduction*, Pro-

ceedings of the National Acadademy of Sciences **105**, 6626-6631 (2008).

[71] N. Wang, J. D. Tytell and D. E. Ingber, *Mechanotransduction at a distance: mechanically coupling the extracellular matrix with the nucleus*, Nature Reviews Molecular Cell Biology **10**, 75–82 (2009).

[72] G. Shivashankar, *Mechanosignaling to the Cell Nucleus and Gene Regulation*, Annual Review of Biophysics **40**, 361–378 (2011).

[73] M. P. Murrell and M. L. Gardel, *F-actin buckling coordinates contractility and severing in a biomimetic actomyosin cortex*, Proceedings of the National Academy of Sciences **109**, 20820–20825 (2012).

[74] P. Müller and J. Kierfeld, *Wrinkling of random and regular semiflexible polymer networks*, Physical Review Letters **112**, 094303 (2014).

[75] O. U. Salman, G. Vitale and L. Truskinovsky, *Continuum theory of bending-to-stretching transition*, Physical Review E **100**, 051001 (2019).

[76] G. A. Buxton and N. Clarke, *"Bending to stretching" transition in disordered networks*, Physical Review Letters **98**, 238103 (2007).

[77] C. P. Broedersz and F. C. MacKintosh, *Modeling semiflexible polymer networks*, Reviews of Modern Physics **86**, 995 (2014).

[78] E. Lerner and E. Bouchbinder, *Scaling theory of critical strain-stiffening in disordered elastic networks*, Extreme Mechanics Letters **65**, 102104 (2023).

[79] N. Parvez, J. Merson and R. C. Picu, *Stiffening mechanisms in stochastic athermal fiber networks*, Physical Review E **108**, 044502 (2023).

[80] M. Briane and G. A. Francfort, *A Two-Dimensional Labile Aether Through Homogenization*, Communications in Mathematical Physics **367**, 599-628 (2019).

[81] G. W. Milton and A. V. Cherkaev, *Which elasticity tensors are realisable?*, Journal of Engineering Materials and Technology **117**, 483–493 (1995).

[82] M. Czajkowski, C. Coulais, M. van Hecke and D. Z. Rocklin, *Conformal elasticity of mechanism-based metamaterials*, Nature Communications **13**, 211 (2022).

[83] A. N. Norris, *Pentamode lattice structures*, In A. S. Phani and M. I. Hussein (Eds), Dynamics of Lattice Materials, John Wiley and Sons Ltd., 179–198 (2017).

[84] R. F. Almgren, *An anisotropic 3-dimensional structure with Poisson's ratio -1*, Journal of Elasticity **15**, 427–430 (1985).

[85] R. Lakes, *Foam Structures with a Negative Poisson's Ratio*, Science, **235**, 1038–1040, (1987).

[86] K. Sun, A. Souslov, X Mao and T. Lubensky, *Surface phonons, elastic response, and conformal invariance in twisted kagome lattices*, Proceedings of the National Academy of Sciences **109**, 12369 (2012).

[87] S. Ulrich, N. Upadhyaya, B. van Opheusden and V. Vitelli, *Shear shocks in fragile networks*, Proceedings of the National Academy of Sciences of the United States of America **110**, 20929– 20934 (2013).

[88] L. R. Gómez, A. M. Turner, M. van Hecke, and V. Vitelli, *Shocks near jamming*, Physical Review Letters **108**, 058001 (2012).

[89] S. Gutiérrez, *Laminations in Linearized Elasticity: The Isotropic Non-very Strongly Elliptic Case*, Journal of Elasticity **53**, 215–256, (1999).

[90] J. Huang, J. Zhang, D. Xu, S. Zhang, H. Tong and N. Xu,*From jammed solids to mechanical metamaterials: A brief review*, Current Opinion in Solid State and Materials Science **27**, 101053 (2023).

[91] M. Manti, V. Cacucciolo and M. Cianchetti, *Stiffening in soft robotics: A review of the state of the art*, IEEE Robotics and Automation Magazine **23**, 93-106 (2016).

[92] Y. Grabovsky and L. Truskinovsky, *Marginal Material Stability*, Journal of Nonlinear Science **23**, 891 (2013).

[93] X. Mao and T. C. Lubensky, *Maxwell Lattices and Topological Mechanics*, Annual Review of Condensed Matter Physics **9**, 413-433 (2018).

[94] T. Chou and D. R. Nelson, *Dislocation-mediated melting near isostructural critical points*, Physical Review E **53**, 2560 (1996).

[95] C. Scheibner, A. Souslov, D. Banerjee, P. Surówka, W. T. M. Irvine and V. Vitelli, *Odd Elasticity*, Nature Physics **16**, 475–480 (2020).

[96] S. Kartha, J. A. Krumhansl, J. P. Sethna and L. K. Wickham, *Disorder-driven pretransitonal tweed pattern in martensitic transformations*, Physical Review B **52**, 803-822 (1995).

[97] M. Born and K Huang, *Dynamical theory of crystal lattices*, Oxford University Press (1996).

[98] J. K. Knowles and E. Sternberg, *On the failure of ellipticity and the emergence of discontinuous deformation gradients in plane finite elastostatics*, Journal of Elasticity, **8**, 329–379 (1978).

[99] J. Ericksen and R. Toupin, *Implications of Hadamard's conditions for elastic stability with respect to uniqueness theorems*, Canadian Journal of Mathematics, University of Toronto Press **8**, 432-436 (1956).

[100] J. I. Gmitro and L. E. Scriven, *A physicochemical basis for pattern and rhythm*, in Intracellular Transport (pp. 221-255), Academic Press (1966).

[101] B. A. Finlayson and L. E. Scriven, *Convective instability by active stress*, Proceedings of the Royal Society of London. A. Mathematical and Physical Sciences **310**, 183-219 (1969).

[102] K. D. Irvine and B. I. Shraiman, *Mechanical control of growth: ideas, facts and challenges*, Development **144**, 4238-4248 (2017).

[103] A. Ioratim-Uba, T. B. Liverpool and S. Henkes, *Mechano-chemical active feedback generates convergence extension in epithelial tissue*, Physical Review Letters **131**, 238301 (2023).

[104] K. Kanatani, *Distribution of directional data and fabric tensors*, International Journal of Engineering Science **22**, 149-164 (1984).

[105] W. Mirza, M. De Corato, M. Pensalfini, G. Vilanova, A. Torres-Sánchez and M. Arroyo, *Theory of active self-organisation of dense nematic structures in actin gels*, arXiv preprint arXiv:2306.15352 (2023).

[106] S. S. M. Konda, J. N. Brantley, C. W. Bielawski and D. E. Makarov, *Chemical reactions modulated by mechanical stress: extended Bell theory*, The Journal of Chemical Physics **135**, 164103 (2011).

[107] M. Kovács, K. Thirumurugan, P. J. Knight, and J. R. Sellers, *Load-dependent mechanism of nonmuscle myosin 2*, Proceedings of the National Academy of Sciences **104**, 9994–9999 (2007).

[108] M. F. Hagan and A. Baskaran, *Emergent self-organisation in active materials*, Current Opinion in Cell Biology **38**, 74–80 (2016).

[109] F. Backouche, L. Haviv, D. Groswasser and A. Bernheim-Groswasser, *Active gels: dynamics of pat-*

terning and self-organisation, Physical Biology **3**, 264 (2006).

[110] G. I. Bell, *Models for the specific adhesion of cells to cells*, Science **200**, 618–627 (1978).

[111] R. Du, L. Li, J. Ji, and Y. Fan, *Receptor-Ligand Binding: Effect of Mechanical Factors*, International Journal of Molecular Sciences *24*, 9062 (2023).

[112] R. Rana, N. Hopper, F. Sidoroff and W. T. Tysoe, *Critical stresses in mechanochemical reactions*, Chemical Science **13**, 12651–12658 (2022).

[113] F. J. Vernerey, *Mechanics of transient semi-flexible networks: Soft-elasticity, stress relaxation and remodeling*, Journal of the Mechanics and Physics of Solids **160**, 104776 (2022).

[114] A. L. Black, J. M. Lenhardt and S. L. Craig, *From molecular mechanochemistry to stress-responsive materials*, Journal of Materials Chemistry **21**, 1655–1663 (2011).

[115] M. L. Gardel, F. Nakamura, J. Hartwig, J. C. Crocker, T. P. Stossel and D. A. Weitz, *Stress-Dependent Elasticity of Composite Actin Networks as a Model for Cell Behavior*, Physical Review Letters **96**, 088102, (2006).

[116] D. Mizuno, C. Tardin, C. F. Schmidt and F. C. MacKintosh, *Nonequilibrium Mechanics of Active Cytoskeletal Networks*, Science **315**, 370-373 (2007).

[117] O. Chaudhuri, S. H. Parekh and D. A. Fletcher, *Reversible stress softening of actin networks*, Nature **445**, 295–298 (2007).

[118] M. Murrell, P. W. Oakes, M. Lenz and M. L. Gardel, *Forcing cells into shape: the mechanics of actomyosin contractility*, Nature Reviews Molecular Cell Biology **16**, 486–498 (2015).

[119] N. Khalilgharibi et al., *Stress relaxation in epithelial monolayers is controlled by the actomyosin cortex*, Nature Physics **15**, 839–847 (2019).

[120] A. F. Pegoraro, P. Janmey and D. A. Weitz, *Mechanical Properties of the Cytoskeleton and Cells*, Cold Spring Harbour Perspectives in Biology **9**, a022038 (2017).

[121] S. Abe and K. Maruyama, *Dynamic rigidity of F-actin-heavy meromyosin solutions*, Biochimica et Biophysica Acta **243**, 98–101 (1971).

[122] S. Hu, K. Dasbiswas, Z. Guo, Y-H. Tee, V. Thiagarajan, P. Hersen, T-L. Chew, S. A. Safran, R. Zaidel-Bar, and A. D. Bershadsky, *Long-range self-organization of cytoskeletal myosin II filament stacks*, Nature Cell Biology **19**, 133–141 (2017).

[123] S. G. Mikhlin, *The spectrum of a family of operators in the theory of elasticity*, Russian Mathematical Surveys **28**, 45–88 (1973).

[124] P. Broedersz, X. Mao, T. C. Lubensky and F. C. MacKintosh, *Criticality and Isostaticity in Fibre Networks*, Nature Physics **7**, 983–988 (2011).

[125] M. van Hecke, *Jamming of soft particles: geometry, mechanics, scaling and isostaticity*, Journal of Physics:Condensed Matter **22**, 033101 (2009).

[126] R. C. Ball and R. Blumenfeld, *Stress Field in Granular Systems: Loop Forces and Potential Formulation*, Physical Review Letters **88**, 115505 (2002).

[127] R. Blumenfeld, *Stresses in Isostatic Granular Systems and Emergence of Force Chains*, Physical Review Letters **93**, 108301 (2004).

[128] H. C. Simpson and S. J. Spector, *On the failure of the complementing condition and non-uniqueness in linear elastostatics*, Journal of Elasticity **15**, 229-231 (1985).

[129] M. Šilhavý, *The Mechanics and Thermodynamics of Continuous Media*, Springer-Verlag (1997).

[130] J. M. Maloney, D. Nikova, F. Lautenschläger E. Clarke, R. Langer, J. Guck and K. J. Van Vliet, *Mesenchymal Stem Cell Mechanics from the Attached to the Suspended State*, Biophysical Journal **99**, 2479–2487 (2010).

[131] Yu. V. Egorov and E. Sanchez-Palencia, *On ill-posedness of free-boundary problems for highly compressible two-dimensional elastic bodies*, St. Petersburg Math. J. **22**, 913–926 (2011).

[132] A. Ninarello, J. Ruiz-Franco and E. Zaccarelli, *Onset of criticality in hyper-auxetic polymer networks*, Nature Communications **13**, 527 (2022).

[133] Y. Zheng, I. Niloy, P. Celli, I. Tobasco and P. Plucinsky, *Continuum Field Theory for the Deformations of Planar Kirigami*, Physical Review Letters **128**, 208003 (2022).

[134] X. Li and R. V. Kohn, *Some results on the Guest–Hutchinson modes and periodic mechanisms of the Kagome lattice metamaterial*, Journal of the Mechanics and Physics of Solids **178**, 105311 (2023).

[135] G. W. Milton and M. Camar-Eddine, *Near optimal pentamodes as a tool for guiding stress while minimizing compliance in 3d-printed materials: A complete solution to the weak g-closure problem for 3d-printed materials*, Journal of the Mechanics and Physics of Solids **114**, 194-208 (2018).

[136] R. Hedayati, A. M. Leeflang and A. A. Zadpoor, *Additively manufactured metallic pentamode meta-materials*, Applied Physics Letters **110**(9), (2017).

[137] D. Misseroni, P. P. Pratapa, K. Liu and G. H. Paulino, *Experimental realisation of tunable Poisson's ratio in deployable origami metamaterials*, Extreme Mechanics Letters **53**, 101685 (2022).

[138] C. McMahan, A. Akerson, P. Celli, B. Audoly and C. Daraio, *Effective continuum models for the buckling of non-periodic architected sheets that display quasi-mechanism behaviors*, Journal of the Mechanics and Physics of Solids **166**, 104934 (2022).

[139] R. Lakes, and K.W. Wojciechowski, *Negative compressibility, negative Poisson's ratio, and stability*, Physica status solidi (b), **245**, 545 (2008).

[140] M. S. d'Avila, N. Triantafyllidis and G. Wen, *Localization of deformation and loss of macroscopic ellipticity in microstructured solids*, Journal of the Mechanics and Physics of Solids **97**, 275–298 (2016).

[141] G. Bordiga, L. Cabras, A. Piccolroaz and D. Bigoni, *Dynamics of prestressed elastic lattices: homogenization, instabilities, and strain localization*, Journal of the Mechanics and Physics of Solids **146**, 104198 (2021).

[142] S. Chiriţă, A. Danescu and M Ciarletta, *On the strong ellipticity of the anisotropic linearly elastic materials*, Journal of Elasticity **87**, 1–27 (2007).

[143] D. De Tommasi, G. Puglisi and G. Zurlo, *A note on strong ellipticity in two-dimensional isotropic elasticity*, Journal of Elasticity **109**, 67–74 (2012).

[144] L. M. Zubov and A. N. Rudev, *A criterion for the strong ellipticity of the equilibrium equations of an isotropic non-linearly elastic material*, Journal of Applied Mathematics and Mechanics **75**, 432–446 (2011).

[145] W. Thomson (Lord Kelvin), *On the reflexion and refraction of light*, Philosophical Magazine **26**, 414-425 (1888).

[146] E. T. Whittaker, *A History of the Theories of Aether and Electricity*, Longmans, Green, and Co. (1910).

[147] R. J. Knops and L. E. Payne, *Uniqueness Theorems in Linear Elasticity*, Springer-Verlag (1971).

[148] A. Kozhevnikov, *A history of the Cosserat spectrum*, Operator Theory: Advances and Applications **109**, 223–234 (1999).

[149] D. Bigoni and D. Capuani, *Green's function for incremental nonlinear elasticity: shear bands and boundary integral formulation*, Journal of the Mechanics and Physics of Solids **50**, 471–500 (2002).

[150] K. Watanabe, *Integral Transform Techniques for Green's Function*, Springer (2014).

[151] X. Cao, A. Nicolas, D. Trimcev and A. Rosso, *Soft modes and strain redistribution in continuous models of amorphous plasticity: the Eshelby paradigm, and beyond?*, Soft Matter **14**, 3640–3651 (2018).

[152] S. Roux and F. Hild, *On the relevance of mean field to continuum damage mechanics*, International Journal of Fracture **116**, 219–229 (2002).

[153] G. Ouillon and D. Sornette, *Long-range static directional stress transfer in a cracked, nonlinear elastic crust*, Future Generation Computer Systems **22**, 500–520 (2006).

[154] L. Caffarelli, L. Nirenberg and J. Spruck, *The Dirichlet Problem for the Degenerate Monge-Ampère Equation*, Revista Mathemática Iberoamericana **2**, 19-27 (1986).

[155] M. Angelillo, E. Babilio and A. Fortunato, *Singular stress fields for masonry-like vaults*, Continuum Mechanics and Thermodynamics **25**, 423–441 (2013).

[156] G. P. Cherepanov, *On the buckling under tension of a membrane containing holes*, Journal of Applied Mathematics and Mechanics **27**, 405 (1963).

[157] P. Guan, N. S. Trudinger and X-J. Wang, *On the Dirichlet Problem for the Degenerate Monge-Ampère Equations*, Acta Mathemática **182**, 87-104 (1999).

[158] F. Fraternali and G. Carpentieri, *On the Correspondence Between 2D Force Networks and Polyhedral Stress Functions*, International Journal of Space Structures **29**, 145-159 (2014).

[159] A. J. Chorin, *Vorticity and Turbulence (Vol. 103)*, Springer Science and Business Media (2013).

[160] M. P. Brenner, S. Hormoz and A. Pumir, *Potential singularity mechanism for the Euler equations*, Physical Review Fluids **1**, 084503 (2016).

[161] G. Q. Chen, G. M. Slemrod, M. and D. Wang, *Fluids, geometry, and the onset of Navier-Stokes turbulence in three space dimensions*, Physica D: Nonlinear Phenomena **376**, 23–30 (2018).

[162] L. Székelyhidi Jr., *Weak solutions to the incompressible Euler equations with vortex sheet initial data*, Comptes Rendus Mathematique **349**(19-20), 1063–1066 (2011).

[163] A. Acharya, G.-Q. G. Chen, S. Li, M. Slemrod and D. Wang, *Fluids, Elasticity, Geometry, and the Existence of Wrinkled Solutions*, Archive for Rational Mechanics and Analysis **226**, 1009–1060 (2017).

[164] C. De Lellis and L. Székelyhidi Jr., *Weak stability and closure in turbulence*, Philosophical Transactions of the Royal Society A **380**, 20210091 (2022).

[165] R. P. Behringer and B. Chakraborty, *The physics of jamming for granular materials: a review*, Reports on Progress in Physics **82**, 012601 (2018).

[166] J. -P. Bouchaud, *Course 4: Granular Media: Some ideas from statistical physics*, In *Slow Relaxations and nonequilibrium dynamics in condensed matter: Les Houches Session LXXVII, 1-26 July*, Berlin, Heidelberg: Springer Berlin Heidelberg, 131–197, (2004).

[167] J. Heyman, *The stone skeleton*, International Journal of Solids and Structures **2**, 249–279 (1966).

[168] G. Del Piero, *Constitutive equation and compatibility of the external loads for linear elastic masonry-like materials*, Meccanica **24**, 150-162 (1989).

[169] M. Angelillo, *Constitutive relations for no tension materials*, Meccanica **28**, 195–202 (1993).

[170] J. N. Nampoothiri, Y. Wang, K. Ramola, J. Zhang, S. Bhattacharjee and B. Chakraborty, *Emergent elasticity in amorphous solids*, Physical Review Letters *125*, 118002 (2020).

[171] R. Blumenfeld, *Granular solids transmit stress as two-phase composites*, arXiv preprint arXiv:2306.10581 (2023).

[172] K. Kondo, T. Iai, S. Moriguti and T. Murasaki, *Tension-field theory*, In K. Kondo (Editor), Memoirs of the Unifying Study of the Basic Problems in Engineering Sciences by Means of Geometry, Vol. 1,417–441, Tokyo: Gakujutsu Bunken Fukyu-Kai (1955).

[173] D. J. Steigmann, *Tension-field theory*, Proceedings of the Royal Society of London A **429**, 141–173 (1990).

[174] A. Panaitescu, M. Xin, B. Davidovitch, J. Chopin, and A. Kudrolli, *Birth and decay of tensional wrinkles in hyperelastic sheets*, Physical Review E **100**, 053003 (2019).

[175] A. C. Pipkin, *The relaxed energy density for isotropic elastic membranes*, IMA Journal of Applied Mathematics **36**, 85–99 (1986).

[176] I. L. Novak, B. M. Slepchenko, A. Mogilner and L. M. Loew, *Cooperativity between cell contractility and adhesion*, Physical Review Letters **93**, 268109 (2004).

[177] O. Campàs, I. Noordstra and A. S. Yap, *Adherens junctions as molecular regulators of emergent tissue mechanics*, Nature Reviews Molecular Cell Biology **25**, 252–269 (2024).

[178] C. Floyd, H. Levine, C. Jarzynski and G. A. Papoian, *Understanding cytoskeletal avalanches using mechanical stability analysis*, Proceedings of the National Academy of Sciences **118**, e2110239118 (2021).

[179] A. M. Alencar, M. S. Ayres Ferraz, C. Y. Park, E. Millet, X. Trepat, J. J. Fredbergb and J. P. Butler, *Non-equilibrium cytoquake dynamics in cytoskeletal remodeling and stabilization*, Soft Matter **12**, 8506-8511 (2016).

[180] L. Cardamone, A. Laio, V. Torre, R. Shahapure and A. DeSimone, *Cytoskeletal actin networks in motile cells are critically self-organized systems synchronized by mechanical interactions*, Proceedings of the National Academy of Sciences **108**, 13978-13983 (2011).

[181] M. R. Lancia, G. V. Caffarelli and P. Podio-Guidugli, *Null Lagrangians in linear elasticity*, Mathematical Models and Methods in Applied Sciences **5**, 415–42 (1995).

[182] E. Verlinde, *Emergent gravity and the dark universe*, SciPost Physics **2**, 16 (2017).

[183] L. Susskind, *The world as a hologram*, Journal of Mathematical Physics **36**, 6377–6396 (1995).

[184] O. Kučera, J. Gaillard, C. Guérin, M. Théry and L. Blanchoin, *Actin-microtubule dynamic composite forms responsive active matter with memory*, Proceedings of The National Academy of Sciences **119**, e2209522119 (2022).

[185] L. Truskinovsky and A. Vainchtein, *The origin of nucleation peak in transformational plasticity*, Journal of the Mechanics and Physics of Solids **52**, 1421-1446 (2004).

[186] L. Truskinovsky and A. Vainchtein, *Dynamics of martensitic phase boundaries: discreteness, dissipation and inertia*, Continuum Mechanics and Thermodynamics **20**, 97-122 (2008).

[187] M. Epstein, *From Saturated Elasticity to Finite Evolution, Plasticity and Growth*, Mathematics and Mechanics of Solids **7**, 255-282 (2002).

[188] S. Ganguly, P. Nath, J. Horbach, P. Sollich, S. Karmakar and S. Sengupta, *Equilibrium and dynamic pleating of a crystalline bonded network*, The Journal of Chemical Physics **146**, 124501 (2017).

[189] S. Conti, A. DeSimone and G. Dolzmann, *Semisoft elasticity and director reorientation in stretched sheets of nematic elastomers*, Physical Review E **66**, 061710 (2002).

[190] S. A. Silling, *Numerical studies of loss of ellipticity near singularities in an elastic material*, Journal of Elasticity **19**, 213-239 (1988).

[191] Y. Grabovsky and L. Truskinovsky, *Solid Phase Transitions in the Liquid Limit*, Journal of Elasticity, 1-29 (2023).

[192] Y. Grabovsky and L. Truskinovsky, *Explicit relaxation of a two-well Hadamard energy*, Journal of Elasticity **135**, 351-373 (2019).

[193] P. Rosakis, *Ellipticity and deformations with discontinuous gradients in finite elastostatics*, Archive for Rational Mechanics and Analysis **109**, 1–37, (1990).

[194] M. F. Staddon, A. Hernandez, M. J. Bowick, M. Moshe and M. C. Marchetti, *The role of non-affine deformations in the elastic behavior of the cellular vertex model*, Soft Matter **19**, 3080-3091 (2023).

[195] S. M. Fielding, J. O. Cochran, J. Huang, D. Bi and M. C. Marchetti, *Constitutive model for the rheology of biological tissue*, Physical Review E **108**, L042602 (2023).

[196] G. Triguero-Platero, F. Ziebert and L. L. Bonilla, *Coarse-graining the vertex model and its response to shear*, arXiv preprint arXiv:2302.04111 (2023).

[197] D. Grossman and J. F. Joanny, *Instabilities and geometry of growing tissues*, Physical Review Letters **129**, 048102 (2022).

[198] R. Kupferman, B. Maman and M. Moshe, *Continuum mechanics of a cellular tissue model*, Journal of the Mechanics and Physics of Solids **143**, 104085 (2020).

[199] G. Y. Qiu and T. J. Pence, *Loss of ellipticity in plane deformation of a simple directionally reinforced incompressible nonlinearly elastic solid*, Journal of Elasticity **49**, 31-63 (1997).

[200] M. P. Santisi d'Avila, N. Triantafyllidis and G. Wen, *Localization of deformation and loss of macroscopic ellipticity in microstructured solids*, Journal of the Mechanics and Physics of Solids **97**, 275-298 (2016).

[201] K. J. Burns, G. M. Vasil, J. S. Oishi, D. Lecoanet and B. P. Brown, *Dedalus: A Flexible Framework for Numerical Simulations with Spectral Methods*, Physical Review Research **2**, 023068 (2020).

[202] C. Kalaitzidou, G. Grekas, A. Zilian, C. Makridakis and P. Rosakis, *Compressive instabilities enable cell-induced extreme densification patterns in the fibrous extracellular matrix: Discrete model predictions*, PLOS Computational Biology **20**, e1012238 (2024).

[203] R. S. Sopher, S. Goren, Y. Koren, O. Tchaicheeyan and A. Lesman, *Intercellular mechanical signalling in a 3D nonlinear fibrous network model*, Mechanics of Materials **184**, 104739 (2023).

[204] A. Krishna, M. Savinov, N. Ierushalmi, A. Mogilner and K. Keren, *Size-dependent transition from steady contraction to waves in actomyosin networks with turnover*, Nature Physics **20**, 123–134 (2024).

[205] M. O. Magnasco, *Forced thermal ratchets*, Physical Review Letters **71**, 1477 (1993).

[206] R. Sheshka and L. Truskinovsky, *Power-stroke-driven actomyosin contractility*, Physical Review E **89**, 012708 (2014).

[207] W. Wu, R. Xia, G. Qian, Z. Liu, N. Razavi, F. Berto, and H. Gao, *Mechanostructures: Rational mechanical design, fabrication, performance evaluation, and industrial application of advanced structures*, Progress in Materials Science **131**, 101021 (2023).

[208] X. Zheng, X. Guo, and I. Watanabe, *A mathematically defined 3D auxetic metamaterial with tunable mechanical and conduction properties*, Materials and Design **198**, 109313 (2021).

[209] Y. Zhang, L. Sun, X. Ren, X. Y. Zhang, Z., Tao, and Y. M Xie, *Design and analysis of an auxetic metamaterial with tuneable stiffness*, Composite Structures **281**, 114997 (2022).

[210] P. Wang, F. Yang, B. Zheng, P. Li, R. Wang, Y. Li, H. Fan and X. Li, *Breaking the Tradeoffs between Different Mechanical Properties in Bioinspired Hierarchical Lattice Metamaterials*, Advanced Functional Materials, 2305978 (2023).

[211] P. Sinha and T. Mukhopadhyay, *Programmable multiphysical mechanics of mechanical metamaterials*, Materials Science and Engineering: R: Reports **155**, 100745 (2023).

[212] H. Chen, Y. Yao, Y. Liu, J. Leng and W. Bian, *A programmable modular lattice metamaterial with multiple deformations*, Mechanics of Advanced Materials and Structures, 1-12 (2023).

[213] D. M. J. Dykstra and C. Coulais, *Inverse design of multishape metamaterials*, arXiv preprint arXiv:2304.12124 (2023).

[214] J. Veenstra, C. Scheibner, M. Brandenbourger, J. Binysh, A. Souslov, V. Vitelli and C. Coulais, *Adaptive locomotion of active solids*, Nature (2025).

[215] D. Bigoni and P. A. Gourgiotis, *Folding and Faulting of an Elastic Continuum*, Proceedings of the Royal Society of London A **472**, 20160018 (2016).

[216] G. C. Everstine and A. C. Pipkin, *Stress channelling in transversely isotropic elastic composites*, Z. Angew. Math. Phys. **22**, 825–834 (1971).

[217] Y. Tang, S. Chen, M. J. Bowick and D. Bi, *Cell Division and Motility Enable Hexatic Order in Biological Tissues*, Physical Review Letters **132**, 218402 (2024).